

A General Control-Theoretic Approach for Reinforcement Learning: Theory and Algorithms

Wei Qin Chen¹, Mark S. Squillante², Chai Wah Wu², Santiago Paternain¹

¹Department of Electrical, Computer, and Systems Engineering, Rensselaer Polytechnic Institute

²Mathematical Sciences Department, IBM Research

Abstract

We devise a control-theoretic reinforcement learning approach to support direct learning of the optimal policy. We establish various theoretical properties of our approach, such as convergence and optimality of our control-theoretic operator, a new control-policy-parameter gradient ascent theorem, and a specific gradient ascent algorithm based on this theorem. As a representative example, we adapt our approach to a particular control-theoretic framework and empirically evaluate its performance on several classical reinforcement learning tasks, demonstrating significant improvements in solution quality, sample complexity, and running time of our control-theoretic approach over state-of-the-art baseline methods.

Introduction

For many years now, reinforcement learning (RL) has been successful in solving a wide variety of decision making under uncertainty problems (Feng et al. 2024; Shen 2024; McMahan et al. 2024; Zheng et al. 2023). Many different RL approaches, with varying degrees of success, have been developed to address such problems (Kaelbling, Littman, and Moore 1996; Szepesvari 2010; Sutton and Barto 2020). Generally speaking, model-free RL methods (Randlov and Alstrom 1998; Mnih et al. 2013) often suffer from high sample complexity that can require an inordinate amount of samples for some problems, making them unsuitable for various applications where collecting large amounts of data is time-consuming, costly and potentially dangerous for the system and its surroundings (Zhang and Tan 2024; Chen, Subramanian, and Paternain 2024; Peng et al. 2023; Dong et al. 2023; Kumar et al. 2020). On the other hand, model-based RL methods have been successful in demonstrating significantly reduced sample complexity and in outperforming model-free approaches for various decision making under uncertainty problems; see, e.g., (Deisenroth and Rasmussen 2011; Meger et al. 2015). However, such model-based approaches can suffer from the difficulty of learning an appropriate model and from worse asymptotic performance than model-free approaches due to model bias from inherently assuming the learned system dynamics model accurately represents the true system environment; see, e.g., (Atkeson and Santamaria 1997; Schneider 1997; Schaal 1997).

In this paper we propose a novel form of RL that seeks to directly learn an optimal control policy for a general un-

derlying (unknown) dynamical system and to directly apply the corresponding learned optimal control policy within the dynamical system. This general approach is in strong contrast to many traditional model-based RL methods that, after learning the system dynamics model which is often of high complexity and dimensionality, then use this system dynamics model to compute an approximate solution of a corresponding (stochastic) dynamic programming problem, often applying model predictive control; see, e.g., (Nagabandi et al. 2018). Our control-based RL (CBRL) approach instead directly learns the unknown parameters that derive, through control-theoretic means, an optimal control policy function from a family of control policy functions, often of much lower complexity and dimensionality, from which the optimal control policy is directly obtained.

The theoretical foundation and analysis of our CRBL approach is presented within the context of a general Markov decision process (MDP) framework that extends the family of policies associated with the classical Bellman operator to a family of control-policy functions mapping a vector of (unknown) parameters from a corresponding parameter set to a control policy which is optimal under those parameters, and that extends the domain of these control policies from a single state to span across all (or a large subset of) states, with the (unknown) parameter vector encoding global and local information that needs to be learned. Within the context of this MDP framework and our general CBRL approach, we establish theoretical results on convergence and optimality with respect to (w.r.t.) a CBRL contraction operator, analogous to corresponding results for the Bellman operator.

The basic idea of learning a form of a parameterized policy within an MDP framework to reduce sample complexity has been studied in the past. One popular approach along these lines concerns policy gradient methods (Sutton et al. 1999; Sutton and Barto 2020), where gradient ascent of the value function in a space of policies is used, possibly together with projection to obtain an optimal policy (Agarwal et al. 2021). These ideas are further refined in neural network based policy optimization approaches (see, e.g., (Agarwal et al. 2021)) such as TRPO (Schulman et al. 2015) and PPO (Schulman et al. 2017). It is important to note, however, that our CBRL approach is fundamentally different in several important ways. More specifically, we exploit control-theoretic methods to derive the optimal policy in terms of es-

imates of a few (global) parameters and directly learn these unknown parameters in an iterative manner based on observations from applying the optimal control policy for the current estimate of parameters. Meanwhile, within the context of our CBRL approach, we establish a new control-policy-parameter gradient ascent theorem, analogous to the standard policy gradient theorem, together with a corresponding gradient ascent method that comprises an iterative process for directly learning the (unknown) parameter vector.

With its foundation being optimal control, our CBRL approach is particularly suitable for dynamical systems in general and therefore the optimal control of a wide variety of systems. In addition to its established theoretical properties, numerical experiments of various classical decision making under uncertainty tasks demonstrate the effectiveness of our CBRL approach in reducing the number of samples needed, which is a key requirement for the application of learning and decision-making algorithms in real-world systems.

We first present our general CBRL approach and then adapt this approach to a particular control-theoretic framework. Empirical results are presented next, followed by concluding remarks. The appendix provides all proofs, and additional theoretical and experimental details and results.

CBRL Approach

Consider a standard RL framework (see, e.g., (Sutton and Barto 2020; Bertsekas and Tsitsiklis 1996)) in which a decision-making agent interacts with a stochastic environment modeled as an MDP defined over a set of states \mathbb{X} , a set of actions \mathbb{U} , a transition probability kernel \mathbb{P} , and a reward function r mapping state-action pairs to a bounded subset of \mathbb{R} . We denote a probability distribution on \mathbb{U} as \mathbb{W} . The agent seeks to determine a policy $\pi(\cdot|x) : \mathbb{X} \rightarrow \mathbb{W}$ comprising the sequence of control actions u_1, u_2, \dots that maximizes the corresponding discounted infinite-horizon stochastic dynamic programming (sDP) formulation expressed as

$$\max_{u_1, u_2, \dots} \mathbb{E}_{\mathbb{P}} \left[\sum_{t=0}^{\infty} \gamma^t r(x_t, u_t) \right], \quad (1)$$

where $x_t \in \mathbb{X}$ denotes the state of the system at time $t \in \mathbb{Z}_+$, $u_t \in \mathbb{U}$ the control action at time t , $\gamma \in (0, 1)$ the discount factor, and $\mathbb{E}_{\mathbb{P}} := \mathbb{E}_{x_{t+1} \sim \mathbb{P}(\cdot|x_t, u_t)}$ defines expectation w.r.t. the conditional transition probability for the next state $\mathbb{P}(\cdot|x_t, u_t)$. The stationary policy $\pi(\cdot|x) : \mathbb{X} \rightarrow \mathbb{W}$ defines a distribution of available control actions given the current state x , which reduces to a deterministic policy $\pi(\cdot|x) : \mathbb{X} \rightarrow \mathbb{U}$ when the conditional distribution renders a constant action for state x ; with slight abuse of notation, we write policy $\pi(x)$. Let $\mathbb{Q}(\mathbb{X} \times \mathbb{U})$ denote the space of bounded real-valued functions over $\mathbb{X} \times \mathbb{U}$ with supremum norm, and let Π denote the set of all stationary policies. From standard RL theory, define the Bellman operator \mathcal{T}_B on $\mathbb{Q}(\mathbb{X} \times \mathbb{U})$ as

$$\mathcal{T}_B Q(x, u) := r(x, u) + \gamma \mathbb{E}_{\mathbb{P}} \max_{u' \in \mathbb{U}} Q(x', u'), \quad (2)$$

where x' denotes the next state upon transition from x . Let $Q^*(x, u)$, $V^*(x) := \max_{u \in \mathbb{U}} Q^*(x, u)$, and $\pi^*(x) :=$

$\arg \max_{u \in \mathbb{U}} Q^*(x, u)$ denote the optimal action-value function, the optimal value function, and the optimal stationary policy, respectively.

Our CBRL approach consists of exploiting control-theoretic methods to solve the general sDP formulation (1) in terms of the unknown system and control variables, and directly learning these unknown parameters over time through a corresponding iterative solution process. In particular, our general approach considers two key ideas: (i) extending the family of policies Π associated with classical RL to a family of control-policy functions that map a parameter vector p from a parameter set to a control policy that is optimal under the parameter vector p ; and (ii) extending the domain of these control policies from a single state to span across all states in \mathbb{X} , with the parameter vector p encoding both global and local information (e.g., gravity and mass) that is unknown and needs to be learned.

More formally, let \mathbb{S} denote a subset of a metric space serving as the set of parameter vectors, and \mathbb{F} the family of control-policy functions whose elements comprise surjective functions $\mathcal{G} : p \mapsto \mathcal{F}_p$ that map a parameter vector $p \in \mathbb{S}$ to a control policy $\mathcal{F}_p : \mathbb{X} \rightarrow \mathbb{W}$ that is optimal under p . For any $p \in \mathbb{S}$, the control-policy function $\mathcal{G}(\cdot) \in \mathbb{F}$ identifies a specific control policy $\mathcal{F}_p \in \Pi$ that provides the best expected cumulative discounted reward across all states $x \in \mathbb{X}$ from among all control-policy functions in \mathbb{F} . Such control policy mappings $\mathcal{G} : \mathbb{S} \rightarrow \Pi$ derive optimal control policies from vectors in the parameter set \mathbb{S} through control-theoretic methods, with the goal of learning the unknown parameter vector $p \in \mathbb{S}$ through a corresponding iterative solution process. Hence, once the parameter vector is learned with sufficient accuracy, the desired optimal control policy is realized.

In the remainder of this section, we first establish theoretical properties of our CBRL approach and then consider a new form of control-policy-parameter gradient ascent methods and corresponding theoretical properties.

Convergence and Optimality. We consider an analog of the Bellman operator \mathcal{T}_B and related theoretical results on convergence and optimality. For each Q -function $q(x, u) \in \mathbb{Q}(\mathbb{X} \times \mathbb{U})$, define the generic CBRL function $\tilde{q} : \mathbb{X} \times \Pi \rightarrow \mathbb{R}$ as $\tilde{q}(x, \mathcal{F}_p) := q(x, \mathcal{F}_p(x))$ where the control policy \mathcal{F}_p is obtained from the control-policy function \mathcal{G} derived from the parameter vector $p \in \mathbb{S}$, and thus $\tilde{q}(x, \mathcal{F}_p) \in \tilde{\mathbb{Q}}(\mathbb{X} \times \Pi)$ with $\tilde{\mathbb{Q}}(\mathbb{X} \times \Pi)$ denoting the space of bounded real-valued functions over $\mathbb{X} \times \Pi$ with supremum norm. We then define our CBRL operator \mathbf{T} on $\tilde{\mathbb{Q}}(\mathbb{X} \times \Pi)$ as

$$(\mathbf{T}\tilde{q})(x, \mathcal{F}_p) := \sum_{y \in \mathbb{X}} \mathbb{P}(y|x, \mathcal{F}_p) \times \left[r(x, \mathcal{F}_p(x)) + \gamma \sup_{p' \in \mathbb{S}} \tilde{q}(y, \mathcal{F}_{p'}) \right]. \quad (3)$$

Our approach comprises a sequence of steps from the family \mathbb{F} to the control-policy functions $\mathcal{G} \in \mathbb{F}$ to the control policies $\mathcal{F}_p \in \Pi$ to the control action $\mathcal{F}_p(x) \in \mathbb{W}$, upon applying \mathcal{F}_p in state $x \in \mathbb{X}$. We next introduce an important assumption on the richness of the family \mathbb{F} within this sequence of steps.

Assumption 1. *There exist a policy function \mathcal{G} in the family \mathbb{F} and a unique vector p^* in the parameter set \mathbb{S} such that, for any state $x \in \mathbb{X}$, $\pi^*(x) = \mathcal{F}_{p^*}(x) = \mathcal{G}(p^*)(x)$.*

Assumption 1 says that \mathbb{F} is rich enough to include a global policy that coincides with the Bellman operator for each state. We then have the following formal result on the convergence of the operator \mathbf{T} of our CBRL approach and the optimality of this convergence w.r.t. the Bellman equation (Sutton and Barto 2020; Bertsekas and Tsitsiklis 1996).

Theorem 1. (a) *For any $\gamma \in (0, 1)$, the operator \mathbf{T} in (3) is a contraction in the supremum norm. (b) Suppose Assumption 1 holds for the family of policy functions \mathbb{F} and its parameter set \mathbb{S} . Then, our CBRL approach with contraction operator \mathbf{T} achieves the same asymptotically optimal outcome as that of the Bellman operator \mathcal{T}_B .*

From Theorem 1(a), for any function $\tilde{q} \in \tilde{\mathcal{Q}}(\mathbb{X} \times \Pi)$, the iterations $\mathbf{T}^t(\tilde{q})$ converge as $t \rightarrow \infty$ to $\tilde{q}'(x, \mathcal{F}_p)$, the unique fixed point of the operator \mathbf{T} , and $\tilde{q}'(x, \mathcal{F}_p)$ satisfies

$$\tilde{q}'(x, \mathcal{F}_p) = \sum_{y \in \mathbb{X}} \mathbb{P}(y | x, \mathcal{F}_p) \left[r(x, \mathcal{F}_p(x)) + \gamma \sup_{p' \in \mathbb{S}} \tilde{q}'(y, \mathcal{F}_{p'}) \right]. \quad (4)$$

Theorem 1(b) implies that, under the contraction operator \mathbf{T} and Assumption 1, our CBRL approach is optimal by realizing the same unique fixed point of the Bellman operator \mathcal{T}_B . We note, however, that this optimality is achieved with great reduction in the sample complexity due in part to another important difference with standard RL, namely the search of our CBRL approach is across all states $x \in \mathbb{X}$ to find a single optimal parameter vector p that derives a single optimal control-policy function $\mathcal{G} \in \mathbb{F}$ which coincides with the Bellman equation for each state. Iterations w.r.t. our CBRL operator \mathbf{T} then consist of improving the estimates of the parameter vector p while applying the optimal control-policy function \mathcal{G} derived from the current estimate of p .

Before addressing this iterative process within the context of policy gradient methods, we first relax some of the above conditions to consider families \mathbb{F} that do not satisfy Assumption 1 and control-policy functions that map a parameter vector to a control policy whose domain spans across a large subset of states (as opposed to all states) in \mathbb{X} and renders asymptotically optimal (as opposed to globally optimal) rewards. Supposing \mathbb{F} satisfies Assumption 1, consider a sequence of less rich families $\mathbb{F}_1 \subset \dots \subset \mathbb{F}_k \subset \mathbb{F}$ of policy functions $\mathcal{G}^{(i)} \in \mathbb{F}_i$ derived from parameter vectors of the corresponding parameter sets \mathbb{S}_i , and define the operators $\mathbf{T}_i : \tilde{\mathcal{Q}}(\mathbb{X} \times \Pi_i) \rightarrow \tilde{\mathcal{Q}}(\mathbb{X} \times \Pi_i)$ as in (3) for any function $\tilde{q}_i(x, \mathcal{F}_p^{(i)}) \in \tilde{\mathcal{Q}}(\mathbb{X} \times \Pi_i)$, $i \in [k] := \{1, \dots, k\}$. Then, from Theorem 1, each operator \mathbf{T}_i under parameter set \mathbb{S}_i is a contraction in the supremum norm and converges to the unique fixed point $\tilde{q}'_i(x, \mathcal{F}_p^{(i)})$ that satisfies the corresponding version of (4), for all $x \in \mathbb{X}$ and $p \in \mathbb{S}_i$, $i \in [k]$. We then have the following formal result on the asymptotic optimality of our CBRL approach in such approximate settings.

Theorem 2. *Assume the state and action spaces are compact and \mathcal{F}_p is uniformly continuous for each p . Consider a sequence of families of policy functions $\mathbb{F}_1 \subset \mathbb{F}_2 \subset \dots \subset$*

$\mathbb{F}_{k-1} \subset \mathbb{F}_k$ such that $\bigcup_{i=1}^k \mathbb{F}_i \rightarrow \mathbb{F}$ as $k \rightarrow \infty$, with \mathbb{S} and \mathbb{S}_i respectively denoting the parameter sets corresponding to \mathbb{F} and \mathbb{F}_i , $i \in [k]$. Then, $\sup_{x \in \mathbb{X}} \|\tilde{q}'_k - \tilde{q}'\| \rightarrow 0$ as $k \rightarrow \infty$.

One specific instance of a sequence of the families of policy functions $\mathbb{F}_1 \subset \dots \subset \mathbb{F}_{k-1} \subset \mathbb{F}_k$ in Theorem 2 consists of piecewise-linear control policies of increasing richness (e.g., the class of canonical piecewise-linear functions (Lin and Unbehauen 1992)) w.r.t. finer and finer granularity of the control policy function space converging towards \mathbb{F} .

Control-Policy-Parameter Gradient Ascent. We now return to our CBRL iterative process in the context of policy gradient methods, building on our foregoing results to establish theoretical results analogous to the standard policy gradient theorem that establishes, for policies parameterized by θ , a connection between the gradient of the value function w.r.t. θ and the gradient of the policy action w.r.t. θ . This theoretical result does not apply to our CBRL approach because there is no direct connection between the parameter vector $p \in \mathbb{S}$ and the control policy action. Rather, under CBRL and for any vector p , the control-policy function $\mathcal{G}(p) \in \mathbb{F}$ identifies a particular control policy $\mathcal{F}_p \in \Pi$, and then the policy applied in any state $x \in \mathbb{X}$ yields the action taken.

Recall that the stationary control policy $\mathcal{F}_p : \mathbb{X} \rightarrow \mathbb{W}$ defines a probability distribution over all available control actions $u \in \mathbb{U}$ given the current state $x \in \mathbb{X}$. Define $\mathcal{F}_{p,u}(x)$ to be the element of $\mathcal{F}_p(x)$ corresponding to action u (i.e., $\mathcal{F}_{p,u}(x) := \mathbb{P}[u_t = u | x_t = x, \mathcal{F}_p]$), and correspondingly define $\tilde{q}_u(x, \mathcal{F}_p) := q_u(x, \mathcal{F}_p(x)) := q^p(x, u)$, where the latter denotes the Q -function of the policy \mathcal{F}_p . Let x_0 denote the start state at time $t = 0$ and $\mathbb{P}(x, k | x_0, \mathcal{F}_p)$ the probability of going from state x_0 to state x in k steps under the control policy \mathcal{F}_p . Our general control-policy-parameter gradient result is then formally expressed as follows.

Theorem 3. *Consider a family of control policy functions \mathbb{F} , its parameter set \mathbb{S} with contraction operator \mathbf{T} in the form of (3), and the value function $V_{\mathcal{F}_p}$ under the control policy \mathcal{F}_p . Assuming $\mathcal{F}_{p,u}(x)$ is differentiable w.r.t. \mathcal{F}_p and $\mathcal{F}_p(x)$ is differentiable w.r.t. p , we then have*

$$\nabla_p V_{\mathcal{F}_p}(x_0) = \sum_{x \in \mathbb{X}} \sum_{k=0}^{\infty} \gamma^k \mathbb{P}(x, k | x_0, \mathcal{F}_p) \times \left[\sum_{u \in \mathbb{U}} \frac{\partial \mathcal{F}_{p,u}(x)}{\partial \mathcal{F}_p} \frac{\partial \mathcal{F}_p(x)}{\partial p} \tilde{q}_u(x, \mathcal{F}_p) \right]. \quad (5)$$

The corresponding gradient ascent result for the case of deterministic control policies follows directly from Theorem 3 with the conditional probability distribution $\mathcal{F}_{p,u}(x)$ given by the associated indicator function $\mathbb{I}_{\mathcal{F}_p(x)}(u)$, returning 1 if and only if $u = \mathcal{F}_p(x)$ and zero otherwise.

Following along similar lines of the various forms of policy-gradient ascent methods based on the standard policy gradient theorem, we devise control-policy-parameter gradient ascent methods within the context of our CBRL approach based on Theorem 3. One such gradient ascent method comprises an iterative process for directly learning the unknown parameter vector p of the optimal control pol-

icy w.r.t. the value function $V_{\mathcal{F}_p}$ whose iterations, with step-size η and $\nabla_p V_{\mathcal{F}_p}$ given by (5), proceed according to

$$p_{t+1} = p_t + \eta \nabla_p V_{\mathcal{F}_p}(x_t). \quad (6)$$

Note that standard policy gradient methods are special cases of (6) where the parameter vector p_t is directly replaced by the policy π_t (see, e.g., (Agarwal et al. 2021)).

Adaptation of CBRL Approach

Our general CBRL approach can be adapted to a given control-theoretic framework of interest. As a representative example, we focus in this paper on the control-theoretic framework of linear quadratic regulator (LQR) in which the system dynamics are linear and the objective function is quadratic. More formally, the LQR system dynamics are governed by $\dot{x} = Ax + Bu$ with initial state x_0 , where the parameter vector p_t is contained in the matrices A and B ; and the LQR objective function to be minimized is given by $\int_0^\infty (x_t^\top Q x_t + u_t^\top R u_t) dt$, where the parameter vector p_t may be contained in the matrices Q and R . Here the matrices A and B respectively define the linear system dynamics and linear system control; and the matrices $Q = Q^\top \succeq 0$ and $R = R^\top \succ 0$ respectively define the quadratic system costs and quadratic control costs. From control theory, it is well known that the solution of the corresponding sDP is determined by solving the algebraic Riccati equation (ARE) (Lancaster and Rodman 1995), whose continuous-time version is expressed as

$$A^\top P + PA - PBR^{-1}B^\top P + Q = 0. \quad (7)$$

The optimal control action u_t^* at time t is then obtained from the solution P of the continuous-time ARE (CARE) as $u_t^* = -Kx_t$, where $K = R^{-1}B^\top P$.

Consider our CBRL approach within the context of the LQR control-theoretic framework where at time t the system is in state x_t and the parameter vector estimate is p_t . The optimal (deterministic) control policy is then given by $\mathcal{F}_p(x_t) = -Kx_t$ via the corresponding solution of the CARE (7), together with the change of coordinates $\tilde{x} = x - x^*$ in general when the target x^* is not the origin. We then update the parameter vector according to the iterative process (6) where $\nabla_p V_{\mathcal{F}_p}$ is obtained from (5) of Theorem 3. In particular, the first partial derivative term on the right hand side of (5) is given by the standard policy gradient solution, and the second partial derivative term on the right hand side of (5) is obtained by differentiation of the CARE (7), which in turn renders (Kao and Hennequin 2020)

$$dP\tilde{A} + \tilde{A}^\top dP + (dZ + dZ^\top + dQ + K^\top dRK) = 0, \quad (8)$$

where $\tilde{A} = A - BK$ and $dZ = P(dA - dBK)$.

Our CBRL approach under the LQR control-theoretic framework concerns the linear dynamics $\dot{x} = Ax + Bu$ where A and B contain elements of the unknown parameter vector p . By leveraging known basic information about the LQR control problem at hand, only a relatively small number of unknown parameters need to be learned. For a wide range of applications where state variables are derivatives of

each other w.r.t. time (e.g., position, velocity, acceleration, jerk), the corresponding rows in the A matrix consist of a single 1 and the corresponding rows in B comprise zeros. We exploit this basic information to consider general matrix forms for A and B that reduce the number of unknown parameters to be learned. As a representative illustration, the system dynamics when there are two groups of such variables have the form given by

$$\underbrace{\begin{bmatrix} \frac{dx_1}{dt} \\ \vdots \\ \frac{d^{k_1} x_1}{dt^{k_1}} \\ \frac{dx_2}{dt} \\ \vdots \\ \frac{d^{k_2} x_2}{dt^{k_2}} \end{bmatrix}}_{\dot{x}} = \underbrace{\begin{bmatrix} 0 & 1 & 0 & \cdots & & 0 \\ 0 & 0 & 1 & \cdots & & \\ a_{10} & \cdots & & & & a_{1n} \\ 0 & \cdots & & 0 & 1 & \cdots & 0 \\ 0 & \cdots & & & 0 & 1 & \cdots \\ a_{20} & \cdots & & & & & a_{2n} \end{bmatrix}}_A x + \underbrace{\begin{bmatrix} 0 \\ \vdots \\ b_0 \\ 0 \\ \vdots \\ b_1 \end{bmatrix}}_B u.$$

Experimental Results

In this section, we conduct numerical experiments to evaluate the performance of our CBRL approach adapted to the above LQR control-theoretic framework, as summarized in Algorithm 1 of the appendix. The objective (1) seeks to maximize the expected cumulative discounted reward, or return. Our numerical experiments consider several classical RL tasks from Gymnasium (Towers et al. 2023), including *Cart Pole*, *Lunar Lander (Continuous)*, *Mountain Car (Continuous)*, and *Pendulum*. We compare our CBRL method with three state-of-the-art RL algorithms, namely DQN (Mnih et al. 2013) for discrete actions, DDPG (Lillicrap et al. 2015) for continuous actions and PPO (Schulman et al. 2017), together with a variant of PPO that solely replaces the non-linear policy of PPO with a linear policy (since we know the optimal policy for some of the problems, e.g., *Cart Pole*, is linear). These baselines are selected as the state-of-the-art algorithms for solving the RL tasks under consideration. Experimental details and additional results are provided in the appendix both in general and for each RL task.

Our CBRL approach depends upon the control-theoretic framework to which it is adapted, where we have chosen LQR as a representative example with the understanding that not all RL tasks can be adequately solved using LQR even if the parameter vector p is known. Recall, however, that our CBRL approach allows the domain of the control policies to span a subset of states in \mathbb{X} , thus enabling partitioning of the state space so that properly increased richness w.r.t. finer and finer granularity can provide improved approximations and asymptotic optimality according to Theorem 2, analogous to the class of canonical piecewise-linear approximations (Lin and Unbehauen 1992). While *Cart Pole* and *Lunar Lander* can be directly addressed within the context of LQR, this is not the case for *Mountain Car* and *Pendulum* which require a nonlinear controller. We therefore partition the state space in the case of such RL tasks and consider a corresponding piecewise-LQR controller where the learned parameter vectors may differ or be shared across the partitions.

All parameters of our CBRL approach are randomly initialized uniformly within $(0, 1)$ and then learned using our

control-policy-parameter gradient ascent iteration (6). We consider four sets of initial parameters to validate the robustness of our CBRL approach for each RL task (see appendix).

Cart Pole under CBRL LQR

Cart Pole, as depicted in Fig. 5 of the appendix, consists of a pole connected to a horizontally moving cart with the goal of balancing the pole by applying a force on the cart to the left or right. The state of the system is $x = [s, \dot{s}, \theta, \dot{\theta}]$ in terms of the position of the cart s , the velocity of the cart \dot{s} , the angle of the pole θ , and the angular velocity of the pole $\dot{\theta}$. With upright initialization of the pole on the cart, each episode comprises 200 steps and the problem is considered “solved” upon achieving an average return of 195.

The LQR controller can be used to solve the *Cart Pole* problem provided that all the parameters of the system are known (e.g., mass of cart, mass and length of pole, gravity), where the angle is kept small by our CBRL approach adapted to the LQR framework. We address the problem within the context of our CBRL approach by exploiting the general matrix form for the LQR dynamics given by (15) in the appendix, solely taking into account general physical relationships (e.g., the derivative of the angle of the pole is equivalent to its angular velocity) and laws (e.g., the force can only affect the acceleration), with the unknown parameters $a_0, \dots, a_7, b_0, b_1$ to be learned; refer to Fig. 1(c).

Fig. 1 and Table 1 (appendix) present numerical results for the three state-of-the-art baselines (discrete actions) and our CBRL approach, with each run over five independent random seeds; see Table 2 and Fig. 6 in the appendix for the four sets of initial parameters in (15). Fig. 1(a) – (b), Table 1 and Fig. 6(a) – (b) clearly demonstrate that our CBRL approach provides far superior performance (both mean and std. dev.) over all baselines w.r.t. both the number of episodes and running time, in addition to demonstrating a more stable training process. Fig. 6(c) – (f) illustrates the learning behavior of CBRL parameters given different initialization.

Lunar Lander under CBRL LQR

Lunar Lander (Continuous), as depicted in Fig. 7 of the appendix, is a classical spacecraft trajectory optimization problem with the goal to land softly and fuel-efficiently on a landing pad by applying thrusters to the left, to the right, and upward. The state of the system is $x = [s_x, v_x, s_y, v_y, \theta, \dot{\theta}]$ in terms of the (x, y) positions s_x and s_y , two linear velocities v_x and v_y , angle θ , and angular velocity $\dot{\theta}$. Starting at the top center of the viewport with a random initial force applied to its center of mass, the lander (spacecraft) is subject to gravity, friction and turbulence while surfaces on the “moon” are randomly generated in each episode with the target landing pad centered at $(0, 0)$. The problem is considered “solved” upon achieving an average return of 200.

The LQR controller can be used to solve the *Lunar Lander (Continuous)* problem provided that all parameters of the system are known (e.g., mass of lander, gravity, friction, etc.), where the angle is kept small by our CBRL approach adapted to the LQR framework. We address the problem within the context of our CBRL approach by exploit-

ing the general matrix form for the LQR dynamics given by (16) in the appendix, solely taking into account general physical relationships (akin to *Cart Pole*) and mild physical information from the system state (e.g., the acceleration is independent of the position), with the unknown parameters $a_0, \dots, a_{11}, b_0, b_1, b_2$ to be learned; refer to Fig. 2(c).

Fig. 2 and Table 3 (see appendix) present numerical results for the three state-of-the-art baselines (continuous actions) and our CBRL approach, with each run over five independent random seeds; see Table 4 and Fig. 8 in the appendix for the four sets of initial parameters in (16). Fig. 2(a) – (b), Table 3 and Fig. 8(a) – (b) clearly demonstrate that our CBRL approach provides far superior performance (both mean and std. dev.) over all baselines w.r.t. both the number of episodes and running time, in addition to demonstrating a more stable training process. We note that the baseline algorithms often crash and terminate sooner than the more successful landings of our CBRL approach, resulting in the significantly worse performance exhibited in Fig. 2, Table 3 and Fig. 8. Finally, Fig. 8(c) – 8(f) illustrates the learning behavior of CBRL parameters given different initialization.

Mountain Car under CBRL Piecewise-LQR

Mountain Car (Continuous), as depicted in Fig. 9 of the appendix, consists of the placement of a car in a valley with the goal of accelerating the car to reach the target at the top of the hill on the right by applying a force on the car to the left or right. The system state is $x = [s, v]$ in terms of the position of the car s and the velocity of the car v . With random initialization at the bottom of the valley, the problem is considered “solved” upon achieving an average return of 90.

Recall that the LQR controller is not sufficient to solve the *Mountain Car (Continuous)* problem, even if all the parameters of the system are known (e.g., mass of the car and gravity), because a nonlinear controller is required. Consequently, we consider a piecewise-LQR controller that partitions the state space into two regions (LQR 1 and LQR 2 in Fig. 9 of the appendix). The target state $x^* = [s^*, v^*]$ is selected to be $x^* = [-1.2, 0]$ if $v < 0$ (LQR 1), and to be $x^* = [0.6, 0]$ otherwise (LQR 2), where -1.2 and 0.6 represent the position of the left hill and the right hill, respectively. We address the problem within the context of our CBRL approach by exploiting the general matrix form for the piecewise-LQR dynamics given by (17) in the appendix, solely taking into account general physical relationships and laws, with the unknown parameters a_0, a_1, b_0, c_0 to be learned; refer to Fig. 3(c).

Fig. 3 and Table 5 (see appendix) present numerical results for the three state-of-the-art baselines (continuous actions) and our CBRL approach, with each run over five independent random seeds; refer to Table 6 and Fig. 10 in the appendix for the four sets of initial parameters in (17). Fig. 3(a) – (b), Table 5 and Fig. 10(a) – (b) clearly demonstrate that our CBRL approach provides superior performance (both mean and std. dev.) over all baselines w.r.t. both the number of episodes and running time, in addition to demonstrating a more stable training process. Fig. 10(c) – 10(f) illustrates the learning behavior of CBRL parameters given different initialization.

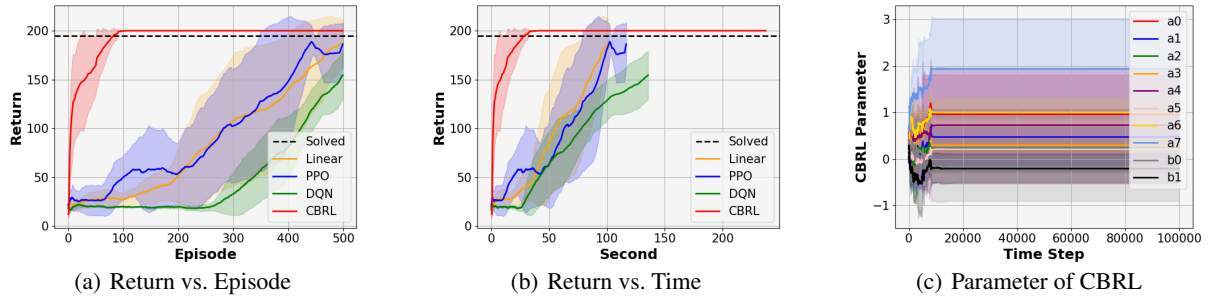


Figure 1: Learning curves of *CartPole-v0* over five independent runs, where the solid line shows the *mean* and the shaded area depicts the *standard deviation*. (a) and (b): Return vs. number of episodes and running time, respectively, for our CBRL approach in comparison with the Linear policy, PPO, and DQN. (c): Learning behavior of CBRL parameters.

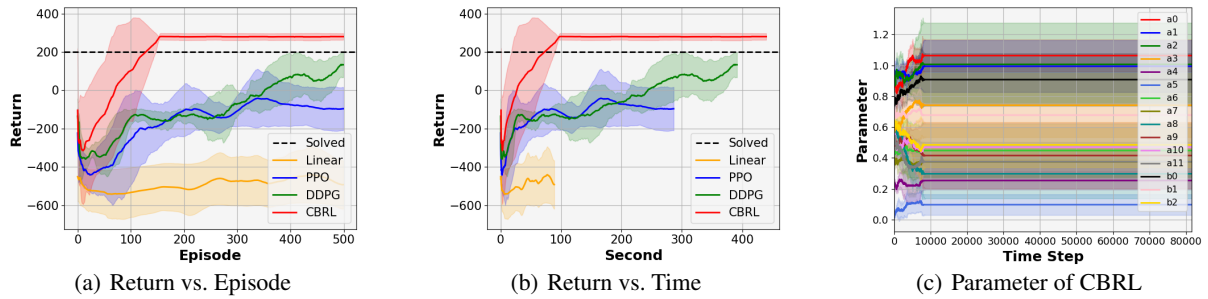


Figure 2: Learning curves of *LunarLanderContinuous-v2* over five independent runs, where the solid line shows the *mean* and the shaded area depicts the *standard deviation*. (a) and (b): Return vs. number of episodes and running time, respectively, for our CBRL approach in comparison with the Linear policy, PPO, and DDPG. (c): Learning behavior of CBRL parameters.

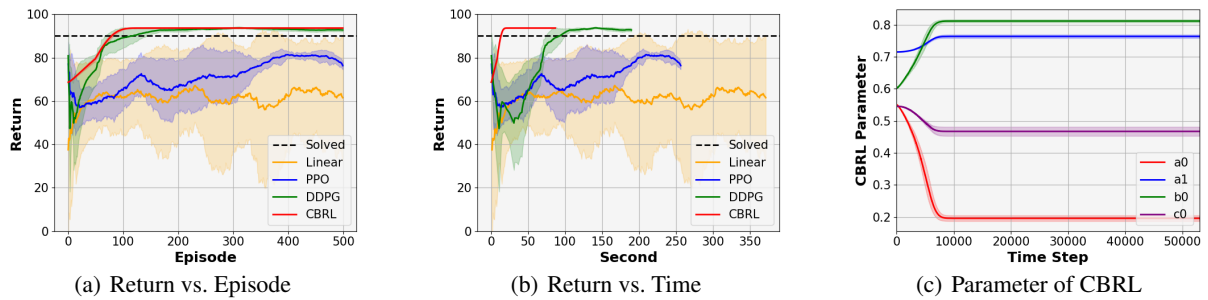


Figure 3: Learning curves of *MountainCarContinuous-v0* over five independent runs, where the solid line shows the *mean* and the shaded area depicts the *standard deviation*. (a) and (b): Return vs. number of episodes and running time, respectively, for our CBRL approach in comparison with the Linear policy, PPO, and DDPG. (c): Learning behavior of CBRL parameters.

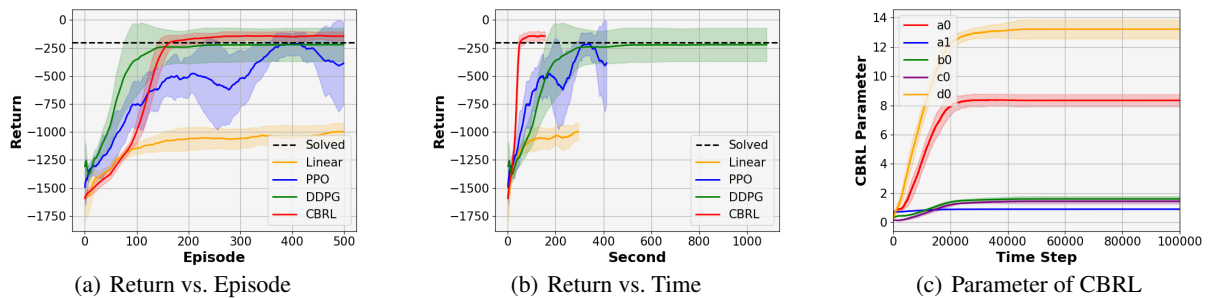


Figure 4: Learning curves of *Pendulum-v1* over five independent runs, where the solid line shows the *mean* and the shaded area depicts the *standard deviation*. (a) and (b): Return vs. number of episodes and running time, respectively, for our CBRL approach in comparison with the Linear policy, PPO, and DDPG. (c): Learning behavior of CBRL parameters.

Pendulum under CBRL Piecewise-LQR

Pendulum, as depicted in Fig. 11 of the appendix, consists of a link attached at one end to a fixed point and the other end being free, with the goal of swinging up to an upright position by applying a torque on the free end. The state of the system is $x = [\theta, \dot{\theta}]$ in terms of the angle of the link θ and the angular velocity of the link $\dot{\theta}$. With random initial link position, each episode comprises 200 steps and the problem is “solved” upon achieving an average return of -200 .

Recall that the LQR controller is not sufficient to solve the *Pendulum* problem, even if all the parameters of the system are known (e.g., mass of the link m , length of the link l , moment of inertia of the link J , and gravity g), because a nonlinear controller is required. Consequently, we consider a piecewise-LQR controller that partitions the state space into four regions (LQR 1 – 4 in Fig. 11 of the appendix). In terms of the target state $x^* = [\theta^*, \dot{\theta}^*]$, the angle θ^* is selected based on the boundary angle in each partition (counter-clockwise boundary angle if $\dot{\theta} > 0$, and clockwise boundary angle otherwise), while the angular velocity $\dot{\theta}^*$ is selected based on the energy conservation law; see the appendix for more details. We address the problem within the context of our CBRL approach by exploiting the general matrix form for the piecewise-LQR dynamics given by (18) in the appendix, solely taking into account general physical relationships and laws, with the unknown parameters a_0, a_1, b_0, c_0, d_0 to be learned; refer to Fig. 4(c).

Fig. 4 and Table 7 (see appendix) present numerical results for the three state-of-the-art baselines (continuous actions) and our CBRL approach, with each run over five independent random seeds; see Table 8 and Fig. 12 in the appendix for the four sets of initial parameters in (18). Fig. 4(a) – (b), Table 7 and Fig. 12(a) – (b) clearly demonstrate that our CBRL approach provides far superior performance (both mean and std. dev.) over all baselines w.r.t. both the number of episodes and running time upon convergence of our CBRL algorithm after a relatively small number of episodes. In particular, even with only four partitions for the difficult nonlinear *Pendulum* RL task, our CBRL approach provides significantly better mean performance, together with a much lower std. dev., than the closest competitor DDPG after 150 episodes. These numerical results also demonstrate a more stable training process for our CBRL approach. Finally, Fig. 12(c) – 12(f) illustrates the learning behavior of CBRL parameters given different initialization.

Discussion

Our results demonstrate an important form of robustness exhibited by the optimal control policy of our CBRL approach w.r.t. the learned parameter values. In particular, we performed additional comparative numerical experiments to evaluate the performance of LQR with the known true parameters for *Cart Pole* and the performance of piecewise-LQR with the known true parameters for *Mountain Car* and *Pendulum* (*Lunar Lander* is omitted because its underlying true parameters are not known to us). We then compare the relative difference between these results for LQR with the true parameters and the corresponding results of our

CBRL approach in Figure 1(a),(b), Figure 3(a),(b), and Figure 4(a),(b). It is important to note that the parameter values learned by our CBRL approach and presented in Figure 1(c), Figure 3(c), and Figure 4(c) differ considerably from the corresponding true parameters. Despite these non-negligible parameter value differences, the comparative relative performance differences for *Cart Pole* and *Pendulum* respectively show that LQR and piecewise-LQR with the true parameters provide no improvement in return over the corresponding return of our CBRL approach in Figure 1(a),(b) and Figure 4(a),(b). In addition, the return of our CBRL approach for *Mountain Car* in Figure 3(a),(b) is within 2% of the corresponding return of piecewise-LQR with the true parameters.

The supremum over the parameter space in the definition of our CBRL operator (3) and its unique fixed point (4) are primarily used for theoretical purposes in this paper. However, one might be concerned about potential computational challenges associated with the supremum when the parameter space is continuous. We first note that this issue is not fundamentally different from the corresponding challenges in standard RL when the action space is continuous, and thus similar steps can be taken to address the issue. Another important factor that mitigates such concerns is the aforementioned robustness of the optimal control policy w.r.t. the learned parameter values. Lastly, we note that this issue did not arise in our numerical experiments using Algorithm 1.

One important implementation issue is stepsize selection, just like in nonconvex optimization and RL. We address this issue by using similar methods employed in standard RL, i.e., the adaptive stepsize selection in our implementation of Algorithm 1. Specifically, we reduce the stepsize η in (6) by a factor of 0.99 each time achieving the “solved” return. Another important implementation issue concerns parameter-vector initialization, again like in nonconvex optimization and RL. As discussed for each of the above RL tasks, the experimental results in Figs. 6, 8, 10, 12 demonstrate the robustness of our CBRL approach w.r.t. parameter-vector initialization. An additional important factor here is the aforementioned robustness of the optimal control policy w.r.t. the learned parameter values. Moreover, given the efficiency of our CBRL approach relative to state-of-the-art methods, additional computations for stepsize selection and parameter-vector initialization can be employed when issues are encountered while retaining overall computational efficiencies.

Conclusion

In this paper we devise a CBRL approach to support direct learning of the optimal policy. We establish various theoretical properties of our approach, including convergence and optimality of our CBRL operator, a new control-policy-parameter gradient ascent theorem, and a gradient ascent algorithm based on this theorem. We then adapt our CBRL approach to the LQR control-theoretic framework, as a representative example, and evaluate its performance on several classical RL tasks. These empirical results demonstrate the significant benefits of our CBRL approach over state-of-the-art baseline methods in terms of improved quality and robustness of the solution and reduced sample complexity and running time.

References

- Agarwal, A.; Kakade, S. M.; Lee, J. D.; and Mahajan, G. 2021. On the Theory of Policy Gradient Methods: Optimality, Approximation, and Distribution Shift. *Journal of Machine Learning Research*, 22(98): 1–76.
- Atkeson, C. G.; and Santamaria, J. C. 1997. A Comparison of Direct and Model-Based Reinforcement Learning. In *Proc. International Conference on Robotics and Automation*.
- Bertsekas, D.; and Tsitsiklis, J. 1996. *Neuro-Dynamic Programming*. Athena Scientific.
- Chen, W.; Subramanian, D.; and Paternain, S. 2024. Probabilistic constraint for safety-critical reinforcement learning. *IEEE Transactions on Automatic Control*.
- Deisenroth, M.; and Rasmussen, C. 2011. PILCO: A model-based and data-efficient approach to policy search. In *Proc. International Conference on Machine Learning*.
- Dong, K.; Flet-Berliac, Y.; Nie, A.; and Brunskill, E. 2023. Model-based offline reinforcement learning with local misspecification. In *Proceedings of the AAAI Conference on Artificial Intelligence*, volume 37, 7423–7431.
- Feng, J.; Feng, M.; Song, H.; Zhou, W.; and Li, H. 2024. SUF: Stabilized Unconstrained Fine-Tuning for Offline-to-Online Reinforcement Learning. In *Proceedings of the AAAI Conference on Artificial Intelligence*, volume 38, 11961–11969.
- Hale, J. K.; and Cruz, M. A. 1970. Existence, uniqueness and continuous dependence for hereditary systems. *Annali di Matematica Pura ed Applicata*, 85: 63–81.
- Kaelbling, L.; Littman, M.; and Moore, A. 1996. Reinforcement Learning: A Survey. *Journal of Artificial Intelligence Research*, 4: 237–285.
- Kao, T.-C.; and Hennequin, G. 2020. Automatic differentiation of Sylvester, Lyapunov, and algebraic Riccati equations. *ArXiv e-prints*.
- Kumar, A.; Zhou, A.; Tucker, G.; and Levine, S. 2020. Conservative q-learning for offline reinforcement learning. *Advances in Neural Information Processing Systems*, 33: 1179–1191.
- Lancaster, P.; and Rodman, L. 1995. *Algebraic Riccati Equations*. Clarendon Press.
- Lillicrap, T. P.; Hunt, J. J.; Pritzel, A.; Heess, N.; Erez, T.; Tassa, Y.; Silver, D.; and Wierstra, D. 2015. Continuous control with deep reinforcement learning. *arXiv preprint arXiv:1509.02971*.
- Lin, J.-N.; and Unbehauen, R. 1992. Canonical piecewise-linear approximations. *IEEE Transactions on Circuits and Systems-I: Fundamental Theory and Applications*, 39(8): 697–699.
- McMahan, J.; Wu, Y.; Zhu, X.; and Xie, Q. 2024. Optimal Attack and Defense for Reinforcement Learning. In *Proceedings of the AAAI Conference on Artificial Intelligence*, volume 38, 14332–14340.
- Meger, D.; Higuera, J.; Xu, A.; Giguere, P.; and Dudek, G. 2015. Learning legged swimming gaits from experience. In *Proc. International Conference on Robotics and Automation*.
- Mnih, V.; Kavukcuoglu, K.; Silver, D.; Graves, A.; Antonoglou, I.; Wierstra, D.; and Riedmiller, R. 2013. Playing Atari with deep reinforcement learning. In *NIPS Workshop on Deep Learning*.
- Nagabandi, A.; Kahn, G.; Fearing, R. S.; and Levine, S. 2018. Neural Network Dynamics for Model-Based Deep Reinforcement Learning with Model-Free Fine-Tuning. In *IEEE International Conference on Robotics and Automation (ICRA)*, 7559–7566.
- Peng, Z.; Han, C.; Liu, Y.; and Zhou, Z. 2023. Weighted policy constraints for offline reinforcement learning. In *Proceedings of the AAAI Conference on Artificial Intelligence*, volume 37, 9435–9443.
- Randlov, J.; and Alstrom, P. 1998. Learning to drive a bicycle using reinforcement learning and shaping. In *Proc. International Conference on Machine Learning*.
- Schaal, S. 1997. Learning From Demonstration. *Advances in Neural Information Processing Systems*.
- Schneider, J. 1997. Exploiting Model Uncertainty Estimates for Safe Dynamic Control Learning. *Advances in Neural Information Processing Systems*.
- Schulman, J.; Levine, S.; Abbeel, P.; Jordan, M.; and Moritz, P. 2015. Trust region policy optimization. In *International conference on machine learning*, 1889–1897. PMLR.
- Schulman, J.; Wolski, F.; Dhariwal, P.; Radford, A.; and Klimov, O. 2017. Proximal policy optimization algorithms. *arXiv preprint arXiv:1707.06347*.
- Shen, K. 2024. Multi-world Model in Continual Reinforcement Learning. In *Proceedings of the AAAI Conference on Artificial Intelligence*, volume 38, 23757–23759.
- Sutton, R. S.; and Barto, A. G. 2020. *Reinforcement Learning: An Introduction*. The MIT Press, second edition.
- Sutton, R. S.; McAllester, D.; Singh, S.; and Mansour, Y. 1999. Policy Gradient Methods for Reinforcement Learning with Function Approximation. In Solla, S.; Leen, T.; and Müller, K., eds., *Advances in Neural Information Processing Systems*, volume 12. MIT Press.
- Szepesvari, C. 2010. Algorithms for Reinforcement Learning. In *Synthesis Lectures on Artificial Intelligence and Machine Learning*, volume 4.1, 1–103. Morgan & Claypool.
- Towers, M.; Terry, J. K.; Kwiatkowski, A.; Balis, J. U.; Cola, G. d.; Deleu, T.; Goulão, M.; Kallinteris, A.; KG, A.; Krimmel, M.; Perez-Vicente, R.; Pierré, A.; Schulhoff, S.; Tai, J. J.; Shen, A. T. J.; and Younis, O. G. 2023. Gymnasium.
- Zhang, Z.; and Tan, X. 2024. An Implicit Trust Region Approach to Behavior Regularized Offline Reinforcement Learning. In *Proceedings of the AAAI Conference on Artificial Intelligence*, volume 38, 16944–16952.
- Zheng, H.; Luo, X.; Wei, P.; Song, X.; Li, D.; and Jiang, J. 2023. Adaptive policy learning for offline-to-online reinforcement learning. In *Proceedings of the AAAI Conference on Artificial Intelligence*, volume 37, 11372–11380.

Control-Based Reinforcement Learning Approach

In this appendix, we present the proofs of our main theoretical results on control-based RL together with additional results and technical details related to our CBRL approach of the main body of the paper. We also present the algorithmic details of our control-policy-parameter gradient ascent method used for our experimental results of the main body of the paper and in the appendix below.

Proof of Theorem 1.

Assumption 1. *There exist a policy function \mathcal{G} in the family \mathbb{F} and a unique vector p^* in the parameter set \mathbb{S} such that, for any state $x \in \mathbb{X}$, $\pi^*(x) = \mathcal{F}_{p^*}(x) = \mathcal{G}(p^*)(x)$.*

Theorem 1. (a) *For any $\gamma \in (0, 1)$, the operator \mathbf{T} in (3) is a contraction in the supremum norm. (b) Suppose Assumption 1 holds for the family of policy functions \mathbb{F} and its parameter set \mathbb{S} . Then, our CBRL approach with contraction operator \mathbf{T} achieves the same asymptotically optimal outcome as that of the Bellman operator \mathcal{T}_B .*

Proof. For the operator \mathbf{T} defined on $\tilde{\mathbb{Q}}(\mathbb{X} \times \Pi)$ in (3) and for any two functions $\tilde{q}_1(x, \mathcal{F}_{p_1}) \in \tilde{\mathbb{Q}}(\mathbb{X} \times \Pi)$ and $\tilde{q}_2(x, \mathcal{F}_{p_2}) \in \tilde{\mathbb{Q}}(\mathbb{X} \times \Pi)$ with $p_1, p_2 \in \mathbb{S}$, we obtain

$$\begin{aligned}
 \|\mathbf{T}\tilde{q}_1 - \mathbf{T}\tilde{q}_2\|_\infty &\stackrel{(a)}{=} \sup_{x \in \mathbb{X}, p \in \mathbb{S}} \left| \sum_{y \in \mathbb{X}} \mathbb{P}(y | x, \mathcal{F}_p) \left[r(x, \mathcal{F}_p(x)) + \gamma \sup_{p_1 \in \mathbb{S}} \tilde{q}_1(y, \mathcal{F}_{p_1}) - r(x, \mathcal{F}_p(x)) - \gamma \sup_{p_2 \in \mathbb{S}} \tilde{q}_2(y, \mathcal{F}_{p_2}) \right] \right| \\
 &\stackrel{(b)}{=} \sup_{x \in \mathbb{X}, p \in \mathbb{S}} \gamma \left| \sum_{y \in \mathbb{X}} \mathbb{P}(y | x, \mathcal{F}_p) \left[\sup_{p_1 \in \mathbb{S}} \tilde{q}_1(y, \mathcal{F}_{p_1}) - \sup_{p_2 \in \mathbb{S}} \tilde{q}_2(y, \mathcal{F}_{p_2}) \right] \right| \\
 &\stackrel{(c)}{\leq} \sup_{x \in \mathbb{X}, p \in \mathbb{S}} \gamma \sum_{y \in \mathbb{X}} \mathbb{P}(y | x, \mathcal{F}_p) \left| \sup_{p_1 \in \mathbb{S}} \tilde{q}_1(y, \mathcal{F}_{p_1}) - \sup_{p_2 \in \mathbb{S}} \tilde{q}_2(y, \mathcal{F}_{p_2}) \right| \\
 &\stackrel{(d)}{\leq} \sup_{x \in \mathbb{X}, p \in \mathbb{S}} \gamma \sum_{y \in \mathbb{X}} \mathbb{P}(y | x, \mathcal{F}_p) \sup_{z \in \mathbb{X}, p' \in \mathbb{S}} |\tilde{q}_1(z, \mathcal{F}_{p'}) - \tilde{q}_2(z, \mathcal{F}_{p'})| \\
 &\stackrel{(e)}{\leq} \sup_{x \in \mathbb{X}, p \in \mathbb{S}} \gamma \sum_{y \in \mathbb{X}} \mathbb{P}(y | x, \mathcal{F}_p) \|\tilde{q}_1 - \tilde{q}_2\|_\infty \\
 &\stackrel{(f)}{=} \gamma \|\tilde{q}_1 - \tilde{q}_2\|_\infty,
 \end{aligned}$$

where (a) is by definition in (3), (b) follows from straightforward algebra, (c) and (d) are due to the triangle inequality, and (e) and (f) directly follow by definition. For any $\gamma \in (0, 1)$, this establishes that the operator \mathbf{T} in (3) is a contraction in the supremum norm, thus rendering the desired result for the first part of the theorem.

For the second part of the theorem, under the stated supposition, we know that the optimal policy $\pi^*(x)$ realized by the Bellman operator holds for a unique vector p^* in the parameter set \mathbb{S} and any $x \in \mathbb{X}$. We also know that the Bellman operator \mathcal{T}_B in (2) and our CBRL operator \mathbf{T} in (3) are both contractions in supremum norm with unique fixed points, where the fixed point of the Bellman operator is the optimal solution of the Bellman equation. In particular, repeatedly applying the Bellman operator \mathcal{T}_B in (2) to an action-value function $q(x, u) \in \mathbb{Q}(\mathbb{X} \times \mathbb{U})$ is well-known to asymptotically yield the unique fixed point equation $\mathcal{T}_B q_B^* = q_B^*$ where

$$q_B^*(x, \pi^*(x)) = \sum_{y \in \mathbb{X}} \mathbb{P}(y | x, \pi^*) \left[r(x, \pi^*(x)) + \gamma \sup_{u' \in \mathbb{U}} q_B^*(y, u') \right] = \sum_{y \in \mathbb{X}} \mathbb{P}(y | x, \pi^*) \left[r(x, \pi^*(x)) + \gamma q_B^*(y, \pi^*(y)) \right], \quad (9)$$

the second equality follows from the definition of $\pi^*(x)$, and q_B^* is the optimal action-value function (Szepesvari 2010). Likewise, repeatedly applying our CBRL operator \mathbf{T} in (3) to an action-value function $\tilde{q}(x, \mathcal{F}_p) \in \tilde{\mathbb{Q}}(\mathbb{X} \times \Pi)$ asymptotically renders the unique fixed point equation $\mathbf{T}\tilde{q}_C^* = \tilde{q}_C^*$ where

$$\tilde{q}_C^*(x, \mathcal{F}_{p^*}) = \sum_{y \in \mathbb{X}} \mathbb{P}(y | x, \mathcal{F}_{p^*}) \left[r(x, \mathcal{F}_{p^*}(x)) + \gamma \sup_{p' \in \mathbb{S}} \tilde{q}_C^*(y, \mathcal{F}_{p'}) \right] = \sum_{y \in \mathbb{X}} \mathbb{P}(y | x, \mathcal{F}_{p^*}) \left[r(x, \mathcal{F}_{p^*}(x)) + \gamma \tilde{q}_C^*(y, \mathcal{F}_{p^*}) \right], \quad (10)$$

and the second equality follows from the relationship between $\tilde{q}(x, \mathcal{F}_{p^*})$ and $\tilde{q}(x, \pi^*)$, given below in (11), under the supposition of the theorem together with the optimality of π^* . By showing that these two fixed points $q_B^*(x, \pi^*(x))$ and $\tilde{q}_C^*(x, \mathcal{F}_{p^*})$ in (9) and (10) coincide, the desired result follows.

To this end, from the definition of $\tilde{q}(x, \mathcal{F}_{p^*})$ and under the stated supposition of the theorem, we have for any $\tilde{q}(x, \mathcal{F}_{p^*}) \in \tilde{\mathbb{Q}}(\mathbb{X} \times \Pi)$ and any $x \in \mathbb{X}$

$$\tilde{q}(x, \mathcal{F}_{p^*}) := q(x, \mathcal{F}_{p^*}(x)) = q(x, \pi^*(x)) =: \tilde{q}(x, \pi^*), \quad (11)$$

noting that p^* is the unique vector in the parameter set \mathbb{S} associated with $\pi^*(x)$. Let $q_C^*(x, \mathcal{F}_{p^*}(x)) = \tilde{q}_C^*(x, \mathcal{F}_{p^*})$ denote the action-value function that corresponds by definition to $\tilde{q}_C^*(x, \mathcal{F}_{p^*})$ of (11) in accordance with (10). Then, in one direction to show $\tilde{q}_C^*(x, \mathcal{F}_{p^*}) \leq q_B^*(x, \pi^*(x))$, we derive

$$\begin{aligned} q_B^*(x, \pi^*(x)) &\stackrel{(a)}{=} \sum_{y \in \mathbb{X}} \mathbb{P}(y | x, \pi^*) \left[r(x, \pi^*(x)) + \gamma q_B^*(y, \pi^*(y)) \right] \\ &\stackrel{(b)}{\geq} \sum_{y \in \mathbb{X}} \mathbb{P}(y | x, \pi^*) \left[r(x, \pi^*(x)) + \gamma q_C^*(y, \pi^*(y)) \right] \stackrel{(c)}{=} \sum_{y \in \mathbb{X}} \mathbb{P}(y | x, \mathcal{F}_{p^*}) \left[r(x, \mathcal{F}_{p^*}(x)) + \gamma q_C^*(y, \mathcal{F}_{p^*}(y)) \right] \\ &\stackrel{(d)}{=} \sum_{y \in \mathbb{X}} \mathbb{P}(y | x, \mathcal{F}_{p^*}) \left[r(x, \mathcal{F}_{p^*}(x)) + \gamma \tilde{q}_C^*(y, \mathcal{F}_{p^*}) \right] \stackrel{(e)}{=} \tilde{q}_C^*(x, \mathcal{F}_{p^*}), \end{aligned} \quad (12)$$

where: (a) is directly from the definition of the fixed point in (9); (b) follows from the definition of the Bellman operator \mathcal{T}_B for any action-value function $q(x, u) \in \mathbb{Q}(\mathbb{X} \times \mathbb{U})$, the unique fixed point (9), and the optimality of q_B^* and π^* ; (c) follows upon the substitution of policy \mathcal{F}_{p^*} for π^* and $q_C^*(x, \pi^*(x)) = q_C^*(x, \mathcal{F}_{p^*}(x))$ from (11); (d) follows upon the substitution of $q_C^*(x, \mathcal{F}_{p^*}(x)) = \tilde{q}_C^*(x, \mathcal{F}_{p^*})$ from (11); and (e) follows from (10). In the other direction to show $q_B^*(x, \pi^*(x)) \leq \tilde{q}_C^*(x, \mathcal{F}_{p^*})$, we derive

$$\begin{aligned} \tilde{q}_C^*(x, \mathcal{F}_{p^*}) &\stackrel{(a)}{=} \sum_{y \in \mathbb{X}} \mathbb{P}(y | x, \mathcal{F}_{p^*}) \left[r(x, \mathcal{F}_{p^*}(x)) + \gamma \tilde{q}_C^*(y, \mathcal{F}_{p^*}) \right] \stackrel{(b)}{=} \sum_{y \in \mathbb{X}} \mathbb{P}(y | x, \mathcal{F}_{p^*}) \left[r(x, \mathcal{F}_{p^*}(x)) + \gamma q_C^*(y, \mathcal{F}_{p^*}(y)) \right] \\ &\stackrel{(c)}{\geq} \sum_{y \in \mathbb{X}} \mathbb{P}(y | x, \mathcal{F}_{p^*}) \left[r(x, \mathcal{F}_{p^*}(x)) + \gamma q_B^*(y, \mathcal{F}_{p^*}(y)) \right] \stackrel{(d)}{=} \sum_{y \in \mathbb{X}} \mathbb{P}(y | x, \pi^*) \left[r(x, \pi^*(x)) + \gamma q_B^*(y, \pi^*(y)) \right] \\ &\stackrel{(e)}{=} q_B^*(x, \pi^*(x)), \end{aligned} \quad (13)$$

where: (a) is directly from the definition of the fixed point in (10); (b) follows upon the substitution of $q_C^*(x, \mathcal{F}_{p^*}(x)) = \tilde{q}_C^*(x, \mathcal{F}_{p^*})$ from (11); (c) follows from the definition of the CBRL operator \mathbf{T} for any action-value function $q(x, u) \in \mathbb{Q}(\mathbb{X} \times \mathbb{U})$, the unique fixed point (10), and the application of the Bellman optimality conditions on \tilde{q}_C^* in (10) for \mathcal{F}_{p^*} , all under the supposition of the theorem; (d) follows upon the substitution of policy π^* for \mathcal{F}_{p^*} and $q_B^*(x, \mathcal{F}_{p^*}(x)) = q_B^*(x, \pi^*(x))$ from (11); and (e) follows from (9). We therefore have coincidence of the fixed points (9) and (10), thus completing the proof. \square

Proof of Theorem 2.

Suppose \mathbb{F} satisfies Assumption 1, and consider a sequence of less rich families $\mathbb{F}_1 \subset \dots \subset \mathbb{F}_k \subset \mathbb{F}$ of policy functions $\mathcal{G}^{(i)} \in \mathbb{F}_i$ derived from parameter vectors of the corresponding parameter sets \mathbb{S}_i , further defining the operators $\mathbf{T}_i : \tilde{\mathbb{Q}}(\mathbb{X} \times \Pi_i) \rightarrow \tilde{\mathbb{Q}}(\mathbb{X} \times \Pi_i)$ as in (3) for any function $\tilde{q}_i(x, \mathcal{F}_p^{(i)}) \in \tilde{\mathbb{Q}}(\mathbb{X} \times \Pi_i)$, $i \in [k] := \{1, \dots, k\}$. From Theorem 1, for $i \in [k]$, we have that the contraction operators $\mathbf{T}_i : \mathbb{Q}(\mathbb{X} \times \Pi_i) \rightarrow \mathbb{Q}(\mathbb{X} \times \Pi_i)$ under the parameter sets \mathbb{S}_i converge to the unique fixed points $\tilde{q}'_i(x, \mathcal{F}_p^{(i)})$ which satisfy, for all $x \in \mathbb{X}$ and $p \in \mathbb{S}_i$,

$$\tilde{q}'_i(x, \mathcal{F}_p^{(i)}) = \sum_{y \in \mathbb{X}} \mathbb{P}(y | x, \mathcal{F}_p^{(i)}) \left[r(x, \mathcal{F}_p^{(i)}(x)) + \gamma \sup_{p' \in \mathbb{S}_i} \tilde{q}'_i(y, \mathcal{F}_{p'}^{(i)}) \right] \quad (14)$$

corresponding to (4). Let us first consider two such families $\mathbb{F}_1 \subset \mathbb{F}_2$, for which we introduce the following lemma used in the proof of Theorem 2.

Lemma 1. *Assume the state and action spaces are compact and \mathcal{F}_p is uniformly continuous for each p . For the two parameter sets \mathbb{S}_1 and \mathbb{S}_2 above and any two parameter vectors $p_1 \in \mathbb{S}_1$ and $p_2 \in \mathbb{S}_2$, let $d(\cdot, \cdot)$ be a sup-norm distance function defined over the action space \mathbb{U} , i.e., $d(\mathcal{F}_{p_1}^{(1)}, \mathcal{F}_{p_2}^{(2)}) = \sup_{x \in \mathbb{X}} \|\mathcal{F}_{p_1}^{(1)}(x) - \mathcal{F}_{p_2}^{(2)}(x)\|$. Then, for all $\epsilon > 0$ there exists $\delta > 0$ such that, if for all $p_1 \in \mathbb{S}_1$ there exists $p_2 \in \mathbb{S}_2$ with $d(\mathcal{F}_{p_1}^{(1)}, \mathcal{F}_{p_2}^{(2)}) < \delta$ and if for all $p_2 \in \mathbb{S}_2$ there exists $p_1 \in \mathbb{S}_1$ with $d(\mathcal{F}_{p_1}^{(1)}, \mathcal{F}_{p_2}^{(2)}) < \delta$, we have $\sup_{x \in \mathbb{X}} \|\tilde{q}'_1 - \tilde{q}'_2\| < \epsilon$.*

Proof. Follows from Lemma 2.2 in (Hale and Cruz 1970), as given in the proof of Theorem 2 below. \square

Intuitively, Lemma 1 shows that, for any policy families $\mathbb{F}_1 \subset \mathbb{F}_2$ sufficiently close to each other, the fixed points \tilde{q}_1 and \tilde{q}_2 of the corresponding operators \mathbf{T}_1 and \mathbf{T}_2 are also close to each other. When the policy families $\mathbb{F}_1 \subset \mathbb{F}_2$ are sufficiently rich and approach \mathbb{F} , then the fixed points of the corresponding operators \mathbf{T}_1 and \mathbf{T}_2 approach the unique fixed point of \mathbb{F} satisfying (4), and therefore they approach the optimal q -value as promised by Bellman from Theorem 1. We formally characterize this asymptotic convergence of approximate optimality to global optimality in Theorem 2.

Theorem 2. Assume the state and action spaces are compact and \mathcal{F}_p is uniformly continuous for each p . Consider a sequence of families of policy functions $\mathbb{F}_1 \subset \mathbb{F}_2 \subset \dots \subset \mathbb{F}_{k-1} \subset \mathbb{F}_k$ such that $\bigcup_{i=1}^k \mathbb{F}_i \rightarrow \mathbb{F}$ as $k \rightarrow \infty$, with \mathbb{S} and \mathbb{S}_i respectively denoting the parameter sets corresponding to \mathbb{F} and \mathbb{F}_i , $i \in [k]$. Then, $\sup_{x \in \mathbb{X}} \|\tilde{q}'_k - \tilde{q}'\| \rightarrow 0$ as $k \rightarrow \infty$.

Proof. First, in the definition of the contraction mapping \mathbf{T} , the result of the supremum depends continuously on the set \mathbb{S} and thus \mathbf{T} depends continuously on \mathbb{S} . Next, since the state and action spaces are compact and \mathcal{F}_p is uniformly continuous for each p , then (Hale and Cruz 1970, Lemma 2.2) shows that the unique fixed point depends continuously on the contraction mapping \mathbf{T} and thus we find that \tilde{q}' depends continuously on the sets \mathbb{S}_i . This implies Lemma 1, from which Theorem 2 then follows directly. \square

Proof of Theorem 3.

Theorem 3. Consider a family of control policy functions \mathbb{F} , its parameter set \mathbb{S} with contraction operator \mathbf{T} in the form of (3), and the value function $V_{\mathcal{F}_p}$ under the control policy \mathcal{F}_p . Assuming $\mathcal{F}_{p,u}(x)$ is differentiable w.r.t. \mathcal{F}_p and $\mathcal{F}_p(x)$ is differentiable w.r.t. p (i.e., both $\partial \mathcal{F}_{p,u}(x)/\partial \mathcal{F}_p$ and $\partial \mathcal{F}_p(x)/\partial p$ exist), we then have

$$\nabla_p V_{\mathcal{F}_p}(x_0) = \sum_{x \in \mathbb{X}} \sum_{k=0}^{\infty} \gamma^k \mathbb{P}(x, k | x_0, \mathcal{F}_p) \times \left[\sum_{u \in \mathbb{U}} \frac{\partial \mathcal{F}_{p,u}(x)}{\partial \mathcal{F}_p} \frac{\partial \mathcal{F}_p(x)}{\partial p} \tilde{q}_u(x, \mathcal{F}_p) \right]. \quad (5)$$

Proof. We derive

$$\begin{aligned} \nabla_p V_{\mathcal{F}_p}(x_0) &\stackrel{(a)}{=} \nabla_p \left[\sum_u \mathcal{F}_{p,u}(x_0) \tilde{q}_u(x_0, \mathcal{F}_p) \right] \\ &\stackrel{(b)}{=} \sum_u [\nabla_p \mathcal{F}_{p,u}(x_0) \tilde{q}_u(x_0, \mathcal{F}_p) + \mathcal{F}_{p,u}(x_0) \nabla_p \tilde{q}_u(x_0, \mathcal{F}_p)] \\ &\stackrel{(c)}{=} \sum_u \left[\nabla_p \mathcal{F}_{p,u}(x_0) \tilde{q}_u(x_0, \mathcal{F}_p) + \gamma \mathcal{F}_{p,u}(x_0) \nabla_p \sum_{x,r} \mathbb{P}(x, r | x_0, \mathcal{F}_p, u) (r + V_{\mathcal{F}_p}(x)) \right] \\ &\stackrel{(d)}{=} \sum_u \left[\nabla_p \mathcal{F}_{p,u}(x_0) \tilde{q}_u(x_0, \mathcal{F}_p) + \gamma \mathcal{F}_{p,u}(x_0) \sum_x \mathbb{P}(x | x_0, \mathcal{F}_p, u) \nabla_p V_{\mathcal{F}_p}(x) \right] \\ &\stackrel{(e)}{=} \sum_u \left[\nabla_p \mathcal{F}_{p,u}(x_0) \tilde{q}_u(x_0, \mathcal{F}_p) + \gamma \mathcal{F}_{p,u}(x_0) \sum_x \mathbb{P}(x | x_0, \mathcal{F}_p, u) \sum_{u'} \left[\nabla_p \mathcal{F}_{p,u'}(x) \tilde{q}_{u'}(x, \mathcal{F}_p) \right. \right. \\ &\quad \left. \left. + \gamma \mathcal{F}_{p,u'}(x) \sum_{x'} \mathbb{P}(x' | x, \mathcal{F}_p, u') \nabla_p V_{\mathcal{F}_p}(x') \right] \right] \\ &\stackrel{(f)}{=} \sum_{x \in \mathbb{X}} \sum_{k=0}^{\infty} \gamma^k \mathbb{P}(x, k | x_0, \mathcal{F}_p) \sum_u \nabla_p \mathcal{F}_{p,u}(x) \tilde{q}_u(x, \mathcal{F}_p), \end{aligned}$$

where (a) is by the definition of the value function for state x_0 , (b) follows from the product rule, (c) follows by the definition of $\tilde{q}_u(x, \mathcal{F}_p)$, (d) follows by applying the gradient w.r.t. p summed over all r , (e) follows by repeating each of the preceding steps for $\nabla_p V_{\mathcal{F}_p}(x')$, and (f) follows from repeated unrolling along the lines of (e) and upon recalling $\mathbb{P}(x, k | x_0, \mathcal{F}_p)$ to be the probability of going from state x_0 to state x in k steps under the control policy \mathcal{F}_p .

The result then follows since $\nabla_p \mathcal{F}_{p,u}(x) = \frac{\partial \mathcal{F}_{p,u}(x)}{\partial \mathcal{F}_p} \frac{\partial \mathcal{F}_p(x)}{\partial p}$, by the chain rule. \square

Control-Policy-Parameter Gradient Ascent Algorithm

Based on our new CBRL gradient ascent theorem (Theorem 3), we devise control-policy-parameter gradient ascent methods within the context of our general CBRL approach. One such gradient ascent method for directly learning the unknown parameter vector p of the optimal control policy w.r.t. the value function V comprises the iterative process according to (6) with stepsize η . Here $\nabla_p V_{\mathcal{F}_p}$ is as given by (5), where the first gradient term $\partial \mathcal{F}_{p,u}(x)/\partial \mathcal{F}_p$ is essentially the standard policy gradient, and the second gradient term $\partial \mathcal{F}_p(x)/\partial p$ is specific to the control-theoretic framework employed in our general CBRL approach; refer to our adaptation of the CBRL approach in the main body of the paper. We note that the standard policy gradient ascent method is a special case of (6) where the parameter vector p is directly replaced by the policy π ; see, e.g., (Agarwal et al. 2021).

Our algorithmic implementation of the above control-policy-parameter gradient ascent method is summarized in Algorithm 1. This algorithm, together with the adaptation of our general CBRL approach to the LQR control-theoretic framework according to the corresponding section of the main body of the paper, is used to obtain the numerical results for our CBRL approach presented in the experimental results of the main body of the paper and in the appendix below.

Algorithm 1: Control-Policy-Parameter Gradient Ascent Algorithm

Require: $\mathcal{E}, \mathbb{X}, \mathbb{U}, \mathbb{F}, \mathcal{F}_p, \mathbf{u}(\cdot, \cdot), D_0 = \Phi, \eta, N$ \triangleright Environment, State Set, Control Action Set, Control-Policy Family, Control-Policy, Control Action Generator (CBRL-LQR), Empty Rollout Dataset, Stepsize, Number of Iterations

Initialize $p_0 \mid \mathcal{F}_{p_0} \in \mathbb{F}, \mathbf{X}_0 \in \mathbb{X}$

for $t = 0, 1, \dots, N$ **do**

1. Generate the control action given the current state and control-policy-parameter

$$\mathbf{u}_t = \mathbf{u}(\mathbf{X}_t, p_t)$$

2. Collect the rollout transition data by applying the control action to the environment \mathcal{E}

$$\mathcal{E} \xrightarrow{\mathbf{u}_t} \mathbf{rollout} := (\mathbf{X}_t, \mathbf{u}_t, r, \mathbf{X}_{t+1})$$

$$D_{t+1} = D_t \cup \mathbf{rollout}$$

3. Compute the control-policy-parameter gradient (5) given the current rollout dataset D_{t+1}
4. Update the control-policy-parameter using the gradient ascent iteration (6)

$$p_{t+1} = p_t + \eta \nabla_p V_{\mathcal{F}_p}(\mathbf{X}_t)$$

end for

Experimental Results

In this appendix we provide additional details and results based on our numerical experiments to evaluate the performance of our CBRL approach adapted to the LQR control-theoretic framework and using Algorithm 1. Recall that we consider the following classical RL tasks from Gymnasium (Towers et al. 2023): *Cart Pole*, *Lunar Lander (Continuous)*, *Mountain Car (Continuous)*, and *Pendulum*. Our CBRL approach is compared against the three state-of-the-art RL algorithms DQN (Mnih et al. 2013) for discrete actions, DDPG (Lillicrap et al. 2015) for continuous actions and PPO (Schulman et al. 2017), together with a variant of PPO that solely replaces the nonlinear policy of PPO with a linear policy (since we know the optimal policy for problems such as *Cart Pole* is linear). These baselines are selected as the state-of-the-art RL algorithms for solving the RL tasks under consideration.

Our CBRL approach depends upon the control-theoretic framework to which it is adapted, where we have chosen LQR as a representative example with the understanding that not all RL tasks can be adequately solved using LQR even if the parameter vector p is known. Recall, however, that our CBRL approach allows the domain of the control policies to span a subset of states in \mathbb{X} , thus enabling the partitioning of the state space so that properly increased richness w.r.t. finer and finer granularity can provide improved approximations and asymptotic optimality according to Theorem 2 in the main body of the paper, analogous to the class of canonical piecewise-linear approximations (Lin and Unbehauen 1992). While *Cart Pole* and *Lunar Lander (Continuous)* can be directly addressed within the context of LQR, this is not the case for *Mountain Car (Continuous)* and *Pendulum* which require a nonlinear controller. We therefore partition the state space in the case of these RL tasks and consider a corresponding piecewise-LQR controller where the learned parameter vectors may differ or be shared across the partitions. Such details are provided below for *Mountain Car (Continuous)* and *Pendulum*.

Cart Pole under CBRL LQR

Environment. As depicted in Figure 5 and described in the main body of the paper, *Cart Pole* consists of a pole connected to a horizontally moving cart with the goal of balancing the pole by applying a force on the cart to the left or right. The state of the system is given by $x = [s, \dot{s}, \theta, \dot{\theta}]$ in terms of the position of the cart s , the velocity of the cart \dot{s} , the angle of the pole θ , and the angular velocity of the pole $\dot{\theta}$.

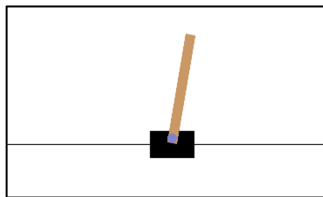


Figure 5: The *CartPole-v0* environment.

Controller. We address the *Cart Pole* problem within the context of our CBRL approach by exploiting the following general matrix form for the LQR dynamics

$$\dot{x} = \begin{bmatrix} \dot{s} \\ \ddot{s} \\ \dot{\theta} \\ \ddot{\theta} \end{bmatrix} = \underbrace{\begin{bmatrix} 0 & 1 & 0 & 0 \\ a_0 & a_1 & a_2 & a_3 \\ 0 & 0 & 0 & 1 \\ a_4 & a_5 & a_6 & a_7 \end{bmatrix}}_A x + \underbrace{\begin{bmatrix} 0 \\ b_0 \\ 0 \\ b_1 \end{bmatrix}}_B u, \quad (15)$$

which solely takes into account general physical relationships (e.g., the derivative of the angle of the pole is equivalent to its angular velocity) and laws (e.g., the force can only affect the acceleration), with the unknown parameters $a_0, \dots, a_7, b_0, b_1$ to be learned.

Numerical Results. Table 1 and Figure 6 present numerical results for the three state-of-the-art baselines (discrete actions) and our CBRL approach, each run over five independent random seeds. All parameters in (15) are initialized uniformly within $(0, 1)$ and then learned using our control-policy-gradient ascent iteration (6). We consider four sets of initial parameters (see Table 2) to validate the robustness of our CBRL approach. Figure 6(c) – 6(f) illustrates the learning behavior of CBRL parameters given different initialization.

Table 1 and Figure 6(a) and 6(b) clearly demonstrate that our CBRL approach provides far superior performance, in terms of both mean and standard deviation, over all baselines w.r.t. both the number of episodes and running time, in addition to demonstrating a more stable training process. More specifically, our CBRL approach outperforms all baselines with a significant improvement in mean return over independent random environment runs from Gymnasium (Towers et al. 2023), together with a significant reduction in the standard deviation of the return over these independent runs, thus rendering a more robust solution

approach where the performance of each run is much closer to the mean than under the corresponding baseline results. In fact, all independent random environment runs under our CBRL approach yield returns equal to the mean (i.e., standard deviation of 0) for episodes 150 and beyond. Moreover, the relative percentage difference¹ in improved mean return performance of our CBRL approach over the next-best RL method Linear (based on mean performance at 500 episodes) is 294% and 6.6% at 200 and 500 episodes, respectively; and the relative percentage difference in reduced standard deviation of return performance from the next-best RL method Linear to our CBRL approach is 200% and 200% at 200 and 500 episodes, respectively. In addition, the relative percentage difference in improved mean return performance of our CBRL approach over the DQN RL method is 927% and 29.5% at 200 and 500 episodes, respectively; and the relative percentage difference in reduced standard deviation of return performance from the DQN RL method to our CBRL approach is 200% and 200% at 200 and 500 episodes, respectively.

We note an important difference between Figure 1(a),(b) and Figure 6(a),(b), namely the shaded areas in Figure 1(a),(b) represent one form of variability across independent random seeds with the same parameter initialization, whereas the shaded areas in Figure 6(a),(b) represent the combination of two forms of variability – one across independent random seeds with the same parameter initialization and the other across different random parameter initializations.

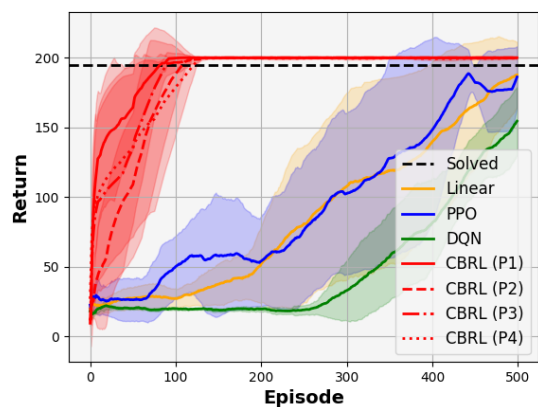
Table 1: Mean and Standard Deviation of Return of RL Methods for *CartPole-v0*

Episode Number	CBRL		Linear		PPO		DQN	
	Mean	Std. Dev.	Mean	Std. Dev.	Mean	Std. Dev.	Mean	Std. Dev.
50	163.49	30.57	27.15	7.79	26.19	15.18	19.99	0.67
100	199.69	0.63	27.05	7.21	49.30	22.28	19.76	1.08
150	200.00	0.00	37.20	14.80	57.84	43.68	18.85	1.23
200	200.00	0.00	50.77	26.93	53.58	32.06	19.47	1.79
250	200.00	0.00	80.05	56.27	75.65	50.67	18.88	3.35
300	200.00	0.00	107.18	67.03	102.31	57.89	32.59	21.07
350	200.00	0.00	118.56	66.73	127.67	71.26	56.44	31.43
400	200.00	0.00	138.79	57.88	147.52	66.20	80.85	31.94
450	200.00	0.00	165.75	45.35	183.12	10.49	123.49	20.59
500	200.00	0.00	187.70	23.72	186.16	22.05	154.46	24.42

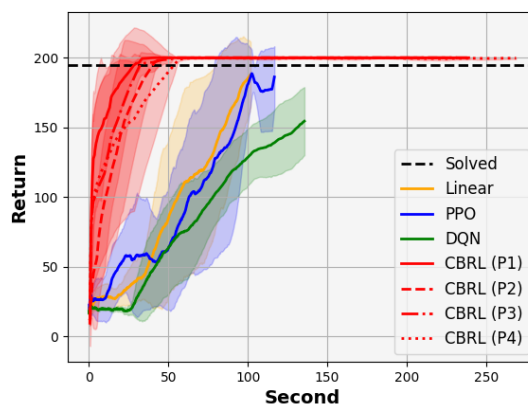
Table 2: Initial Parameters of *CartPole-v0*

Name	a_0	a_1	a_2	a_3	a_4	a_5	a_6	a_7	b_0	b_1
Initial Parameters 1 (P1)	0.436	0.026	0.55	0.435	0.42	0.33	0.205	0.619	0.3	0.267
Initial Parameters 2 (P2)	0.076	0.78	0.438	0.723	0.978	0.538	0.501	0.072	0.268	0.5
Initial Parameters 3 (P3)	0.154	0.74	0.263	0.534	0.015	0.919	0.901	0.033	0.957	0.137
Initial Parameters 4 (P4)	0.295	0.531	0.192	0.068	0.787	0.656	0.638	0.576	0.039	0.358

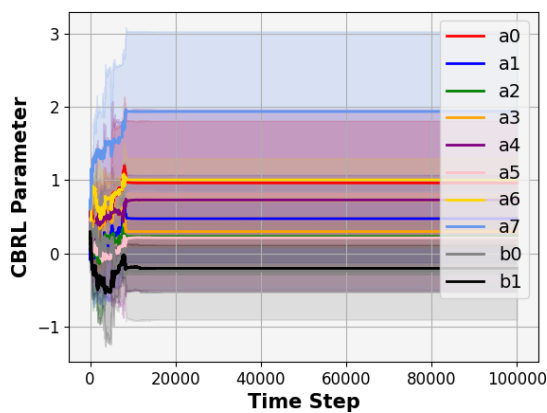
¹For the relative comparison of improved mean return performance of our CBRL method over the next-best RL method, since all the performance values are positive, we use the standard relative percentage difference formula $\frac{M_{CBRL} - M_{RL}}{M_{RL}} \times 100$. Similarly, for the relative comparison of reduced standard deviation of return performance from the next-best RL method to our CBRL method, since all the performance values are positive, we typically use the standard relative percentage difference formula $\frac{S_{RL} - S_{CBRL}}{S_{CBRL}} \times 100$, with the sole exception of replacing the denominator with $(S_{RL} + S_{CBRL})/2$ based on the arithmetic mean when S_{CBRL} is zero. Refer to https://en.wikipedia.org/wiki/Relative_change



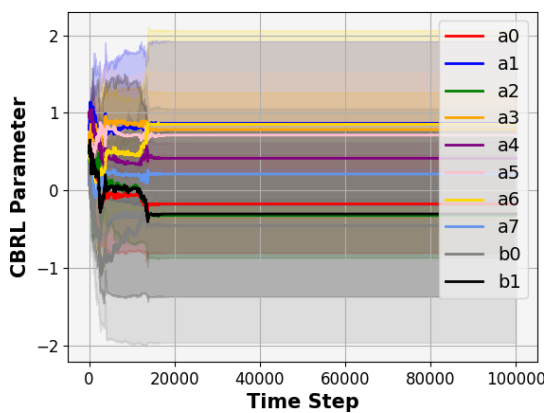
(a) Return vs. Episode



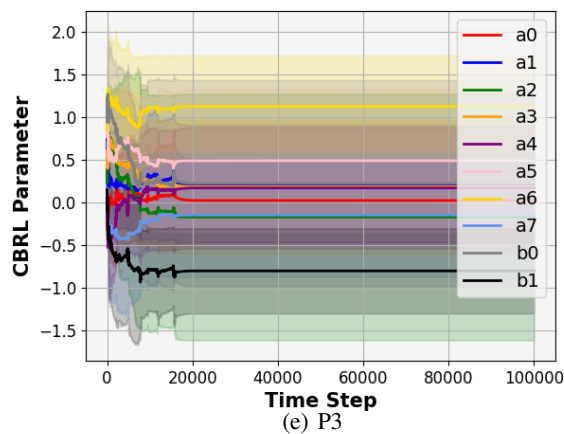
(b) Return vs. Time



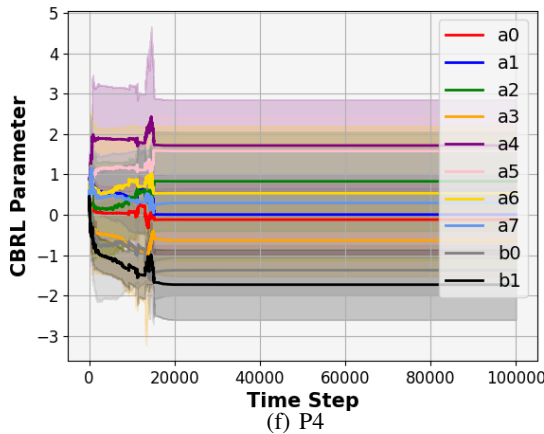
(c) P1



(d) P2



(e) P3



(f) P4

Figure 6: Learning curves of *CartPole-v0* over five independent runs. The solid line shows the mean and the shaded area depicts the standard deviation. (a) and (b): Return vs. number of episodes and running time, respectively, for our CBRL approach (over the five independent runs and the four initializations in Table 2) in comparison with the Linear policy, PPO, and DQN (over the five independent runs). (c) – (f): Learning behavior of CBRL parameters, initialized by Table 2.

Lunar Lander (Continuous) under CBRL LQR

Environment. As depicted in Figure 7 and described in the main body of the paper, *Lunar Lander (Continuous)* is a classical spacecraft trajectory optimization problem with the goal to land softly and fuel-efficiently on a landing pad by applying thrusters to the left, to the right, and upward. The state of the system is given by $x = [s_x, v_x, s_y, v_y, \theta, \dot{\theta}]$ in terms of the (x, y) positions s_x and s_y , two linear velocities v_x and v_y , angle θ , and angular velocity $\dot{\theta}$.

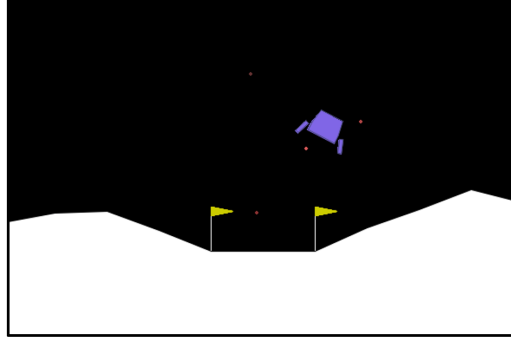


Figure 7: The *LunarLanderContinuous-v2* environment.

Controller. We address the *Lunar Lander (Continuous)* problem within the context of our CBRL approach by exploiting the following general matrix form for the LQR dynamics

$$\dot{x} = \begin{bmatrix} v_x \\ \ddot{s}_x \\ v_y \\ \ddot{s}_y \\ \dot{\theta} \\ \ddot{\theta} \end{bmatrix} = \underbrace{\begin{bmatrix} 0 & 1 & 0 & 0 & 0 & 0 \\ 0 & a_0 & 0 & a_1 & a_2 & a_3 \\ 0 & 0 & 0 & 1 & 0 & 0 \\ 0 & a_4 & 0 & a_5 & a_6 & a_7 \\ 0 & 0 & 0 & 0 & 0 & 1 \\ 0 & a_8 & 0 & a_9 & a_{10} & a_{11} \end{bmatrix}}_A x + \underbrace{\begin{bmatrix} 0 & 0 \\ 0 & b_0 \\ 0 & 0 \\ b_1 & 0 \\ 0 & 0 \\ 0 & b_2 \end{bmatrix}}_B u, \quad (16)$$

which solely takes into account general physical relationships (akin to *Cart Pole*) and mild physical information from the system state (e.g., the acceleration is independent of the position), with the unknown parameters $a_0, \dots, a_{11}, b_0, b_1, b_2$ to be learned.

Numerical Results. Table 3 and Figure 8 present numerical results for the three state-of-the-art baselines (continuous actions) and our CBRL approach, each run over five independent random seeds. All parameters in (16) are initialized uniformly within $(0, 1)$ and then learned using our control-policy-parameter gradient ascent iteration (6). We consider four sets of initial parameters (see Table 4) to validate the robustness of our CBRL approach. Figure 8(c) – 8(f) illustrates the learning behavior of CBRL parameters given different initialization.

Table 3 and Figure 8(a) and 8(b) clearly demonstrate that our CBRL approach provides far superior performance, in terms of both mean and standard deviation, over all baselines w.r.t. both the number of episodes and running time, in addition to demonstrating a more stable training process. More specifically, our CBRL approach outperforms all baselines with a significant improvement in mean return over independent random environment runs from Gymnasium (Towers et al. 2023), together with a significant reduction in the standard deviation of the return over these independent runs, thus rendering a more robust solution approach where the performance of each run is much closer to the mean than under the corresponding baseline results. In fact, the relative percentage difference² in improved mean return performance of our CBRL approach over the next-best RL method DDPG (based on mean performance at 500 episodes) is 309% and 110% at 200 and 500 episodes, respectively; and the relative percentage difference in reduced standard deviation of return performance from the next-best RL method DDPG to our CBRL approach is 115% and 288% at 200 and 500 episodes, respectively. Moreover, the relative percentage difference in improved

²For the relative comparison of improved mean return performance of our CBRL method over the next-best RL method, since some of the performance values are negative and $|M_{RL}| < M_{CBRL}$, we use the standard relative percentage difference formula $\frac{M_{CBRL} - M_{RL}}{|M_{RL}|} \times 100$. Similarly, for the relative comparison of reduced standard deviation of return performance from the next-best RL method to our CBRL method, since all the performance values are positive, we use the standard relative percentage difference formula $\frac{S_{RL} - S_{CBRL}}{S_{CBRL}} \times 100$. Refer to https://en.wikipedia.org/wiki/Relative_change

mean return performance of our CBRL approach over the PPO RL method is 361% and 390% at 200 and 500 episodes, respectively; and the relative percentage difference in reduced standard deviation of return performance from the PPO RL method to our CBRL approach is 639% and 559% at 200 and 500 episodes, respectively. We note that the baseline algorithms often crash and terminate sooner than the more successful landings of our CBRL approach, resulting in the significantly worse performance exhibited in Figure 2, Table 3 and Figure 8.

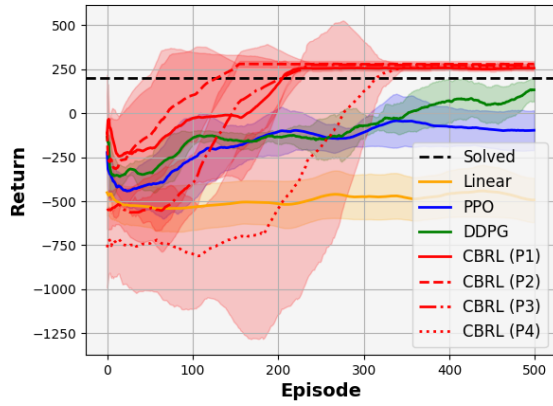
We also note an important difference between Figure 2(a),(b) and Figure 8(a),(b), namely the shaded areas in Figure 2(a),(b) represent one form of variability across independent random seeds with the same parameter initialization, whereas the shaded areas in Figure 8(a),(b) represent the combination of two forms of variability – one across independent random seeds with the same parameter initialization and the other across different random parameter initializations.

Table 3: Mean and Standard Deviation of Return of RL Methods for *LunarLanderContinuous-v2*

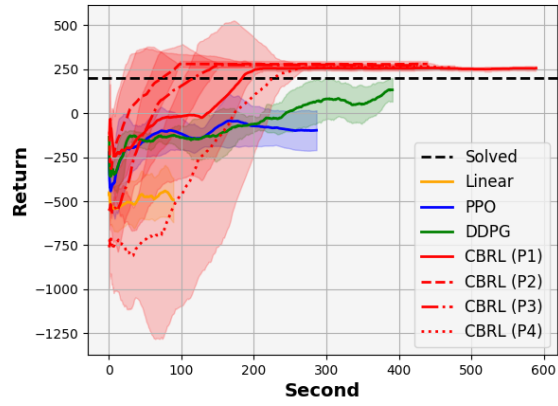
Episode Number	CBRL		Linear		PPO		DDPG	
	Mean	Std. Dev.	Mean	Std. Dev.	Mean	Std. Dev.	Mean	Std. Dev.
50	-128.81	276.58	-531.05	115.63	-403.56	143.06	-337.22	98.64
100	101.33	262.09	-533.6	130.04	-260.08	238.84	-145.05	42.29
150	258.84	31.52	-510.13	123.56	-188.50	121.78	-154.48	43.2
200	279.24	18.12	-513.44	129.48	-106.87	133.97	-133.51	38.96
250	280.36	17.19	-475.43	125.81	-127.29	81.82	-143.46	112.20
300	279.19	18.42	-473.77	127.78	-109.72	79.65	-73.1	70.24
350	280.08	17.14	-479.01	124.67	-45.12	140.02	-9.04	98.49
400	279.51	17.67	-458.10	131.61	-75.52	111.54	70.04	120.93
450	278.96	19.22	-445.52	143.65	-91.77	105.02	51.15	99.21
500	280.09	17.16	-492.67	126.01	-96.50	113.10	133.20	66.54

Table 4: Initial Parameters of *LunarLanderContinuous-v2*

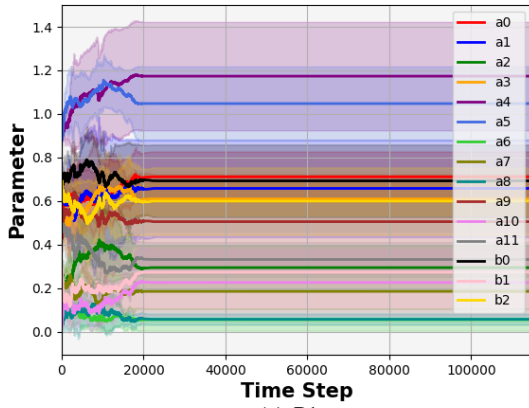
Name	a_0	a_1	a_2	a_3	a_4	a_5	a_6	a_7
Initial Parameters 1 (P1)	0.551	0.708	0.291	0.511	0.893	0.896	0.126	0.207
Initial Parameters 2 (P2)	0.873	0.969	0.869	0.531	0.233	0.011	0.43	0.402
Initial Parameters 3 (P3)	0.778	0.238	0.824	0.966	0.973	0.453	0.609	0.776
Initial Parameters 4 (P4)	0.65	0.505	0.879	0.182	0.852	0.75	0.666	0.988
Name	a_8	a_9	a_{10}	a_{11}	b_0	b_1	b_2	
Initial Parameters 1 (P1)	0.051	0.441	0.03	0.457	0.649	0.278	0.676	
Initial Parameters 2 (P2)	0.523	0.478	0.555	0.543	0.761	0.712	0.62	
Initial Parameters 3 (P3)	0.642	0.722	0.035	0.298	0.059	0.857	0.373	
Initial Parameters 4 (P4)	0.257	0.028	0.636	0.847	0.736	0.021	0.112	



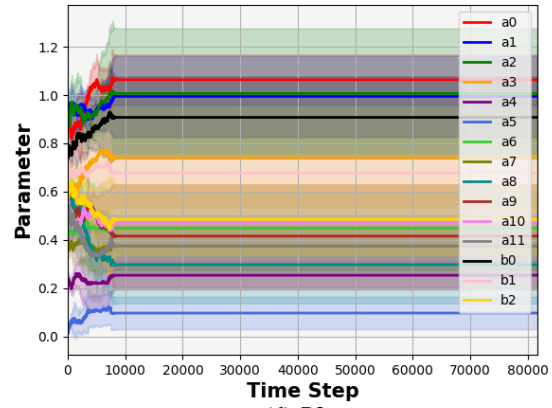
(a) Return vs. Episode



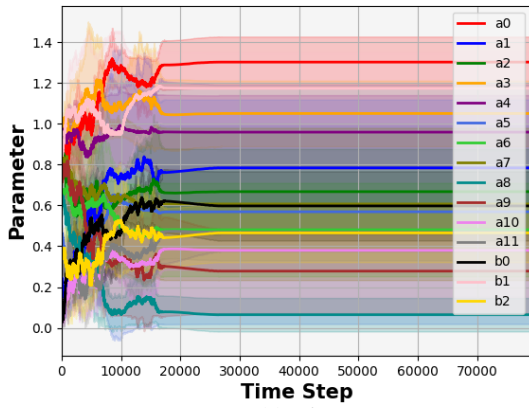
(b) Return vs. Time



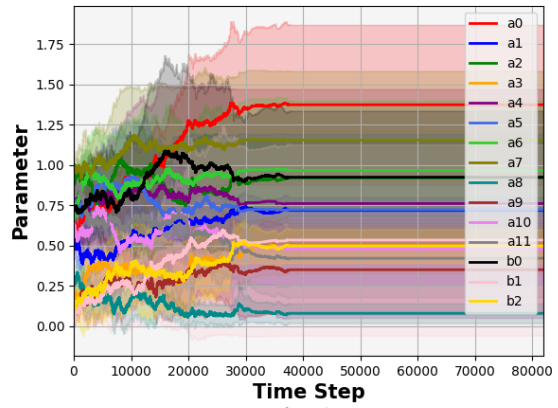
(c) P1



(d) P2



(e) P3



(f) P4

Figure 8: Learning curves of *LunarLanderContinuous-v2* over five independent runs. The solid line shows the mean and the shaded area depicts the standard deviation. (a) and (b): Return vs. number of episodes and running time, respectively, for our CBRL approach (over the five independent runs and the four initializations in Table 4) in comparison with the Linear policy, PPO, and DDPG (over the five independent runs). (c) – (f): Learning behavior of CBRL parameters, initialized by Table 4.

Mountain Car (Continuous) under CBRL Piecewise-LQR

Environment. As depicted in Figure 9 and described in the main body of the paper, *Mountain Car (Continuous)* consists of a car placed in a valley with the goal of accelerating the car to reach the target at the top of the hill on the right by applying a force on the car to the left or right. The state of the system is given by $x = [s, v]$ in terms of the position of the car s and the velocity of the car v .

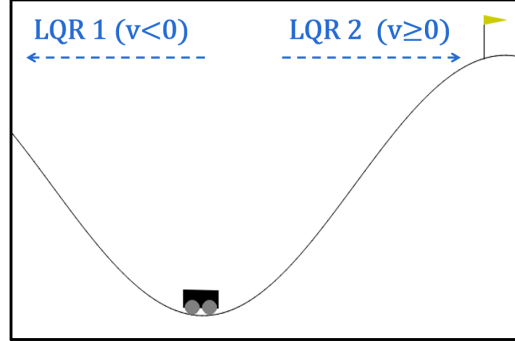


Figure 9: The *MountainCarContinuous-v0* environment and partitions for piecewise-LQR.

Controller. Recall that the LQR controller is not sufficient to solve the *Mountain Car (Continuous)* problem, even if all the parameters of the system are known (e.g., mass of the car and gravity), because a nonlinear controller is required. Consequently, we consider a piecewise-LQR controller that partitions the state space into two regions: LQR 1 and LQR 2 (see Figure 9). The target state $x^* = [s^*, v^*]$ for LQR 1 and LQR 2 are respectively selected as $x^* = [-1.2, 0]$ and $x^* = [0.6, 0]$, where -1.2 and 0.6 correspondingly represent the position of the left hill and the right hill. We address the problem within the context of our CBRL approach by exploiting the following general matrix form for the piecewise-LQR dynamics

$$\dot{e} = \begin{bmatrix} v - v^* \\ \dot{v} - \dot{v}^* \end{bmatrix} = \begin{bmatrix} 0 & 1 \\ a_0 \sin(3s^*) & a_1 \end{bmatrix} e + \begin{bmatrix} 0 \\ b_0 \end{bmatrix} (u - c_0 \cos(3s^*)), \quad (17)$$

which solely takes into account general physical relationships and laws, with the unknown parameters a_0, a_1, b_0, c_0 to be learned where $e = x - x^*$ and we select $v^* = 0, \dot{v}^* = 0$, and $s^* = -1.2$ or 0.6 .

Numerical Results. Table 5 and Figure 10 present numerical results for the three state-of-the-art baselines (continuous actions) and our CBRL approach, each run over five independent random seeds. All parameters in (17) are initialized uniformly within $(0, 1)$ and then learned using our control-policy-parameter gradient ascent iteration (6). We consider four sets of initial parameters (see Table 6) to validate the robustness of our CBRL approach. Figure 10(c) – 10(f) illustrates the learning behavior of CBRL parameters given different initialization.

Table 5 and Figure 10(a) and 10(b) clearly demonstrate that our CBRL approach provides superior performance, in terms of both mean and standard deviation, over all baselines w.r.t. both the number of episodes and running time, in addition to demonstrating a more stable training process. More specifically, our CBRL approach outperforms all baselines with a significant improvement in mean return over independent random environment runs from Gymnasium (Towers et al. 2023), together with a significant reduction in the standard deviation of the return over these independent runs, thus rendering a more robust solution approach where the performance of each run is much closer to the mean than under the corresponding baseline results. In fact, the relative percentage difference³ in improved mean return performance of our CBRL approach over the next-best RL method DDPG (based on mean performance at 500 episodes) is 0.9% and 1% at 200 and 500 episodes, respectively; and the relative percentage difference in reduced standard deviation of return performance from the next-best RL method DDPG to our CBRL approach is 324% and 257% at 200 and 500 episodes, respectively. Moreover, the relative percentage difference in improved mean return performance of our CBRL approach over the PPO RL method is 41% and 23% at 200 and 500 episodes, respectively; and the relative percentage difference in reduced standard deviation of return performance from the PPO RL method to our CBRL approach is 5743% and 729% at 200 and 500 episodes, respectively.

³For the relative comparison of improved mean return performance of our CBRL method over the next-best RL method, since all the performance values are positive, we use the standard relative percentage difference formula $\frac{M_{CBRL} - M_{RL}}{M_{RL}} \times 100$. Similarly, for the relative comparison of reduced standard deviation of return performance from the next-best RL method to our CBRL method, since all the performance values are positive, we use the standard relative percentage difference formula $\frac{S_{RL} - S_{CBRL}}{S_{CBRL}} \times 100$. Refer to https://en.wikipedia.org/wiki/Relative_change

We note an important difference between Figure 3(a),(b) and Figure 10(a),(b), namely the shaded areas in Figure 3(a),(b) represent one form of variability across independent random seeds with the same parameter initialization, whereas the shaded areas in Figure 10(a),(b) represent the combination of two forms of variability – one across independent random seeds with the same parameter initialization and the other across different random parameter initializations.

Table 5: Mean and Standard Deviation of Return of RL Methods for *MountainCarContinuous-v0*

Episode Number	CBRL		Linear		PPO		DDPG	
	Mean	Std. Dev.	Mean	Std. Dev.	Mean	Std. Dev.	Mean	Std. Dev.
50	79.34	1.02	61.09	16.84	59.62	7.32	74.20	7.20
100	93.03	0.37	61.64	17.19	65.01	9.69	89.10	4.78
150	93.63	0.21	63.12	19.53	69.58	10.57	91.98	1.47
200	93.63	0.21	61.94	21.83	66.36	12.27	92.82	0.89
250	93.63	0.21	62.30	25.59	71.35	13.15	93.18	0.41
300	93.63	0.21	62.00	25.12	71.25	12.27	93.62	0.35
350	93.63	0.21	57.13	34.55	76.23	3.03	93.39	0.51
400	93.63	0.21	62.42	25.91	81.32	1.63	93.15	0.81
450	93.63	0.21	66.19	20.54	81.10	2.02	92.67	0.85
500	93.63	0.21	61.52	28.84	76.31	1.74	92.72	0.75

Table 6: Initial Parameters of *MountainCarContinuous-v0*

Name	a_0	a_1	b_0	c_0
Initial Parameters 1 (P1)	0.549	0.715	0.603	0.545
Initial Parameters 2 (P2)	0.222	0.871	0.207	0.919
Initial Parameters 3 (P3)	0.771	0.021	0.634	0.749
Initial Parameters 4 (P4)	0.588	0.898	0.892	0.816

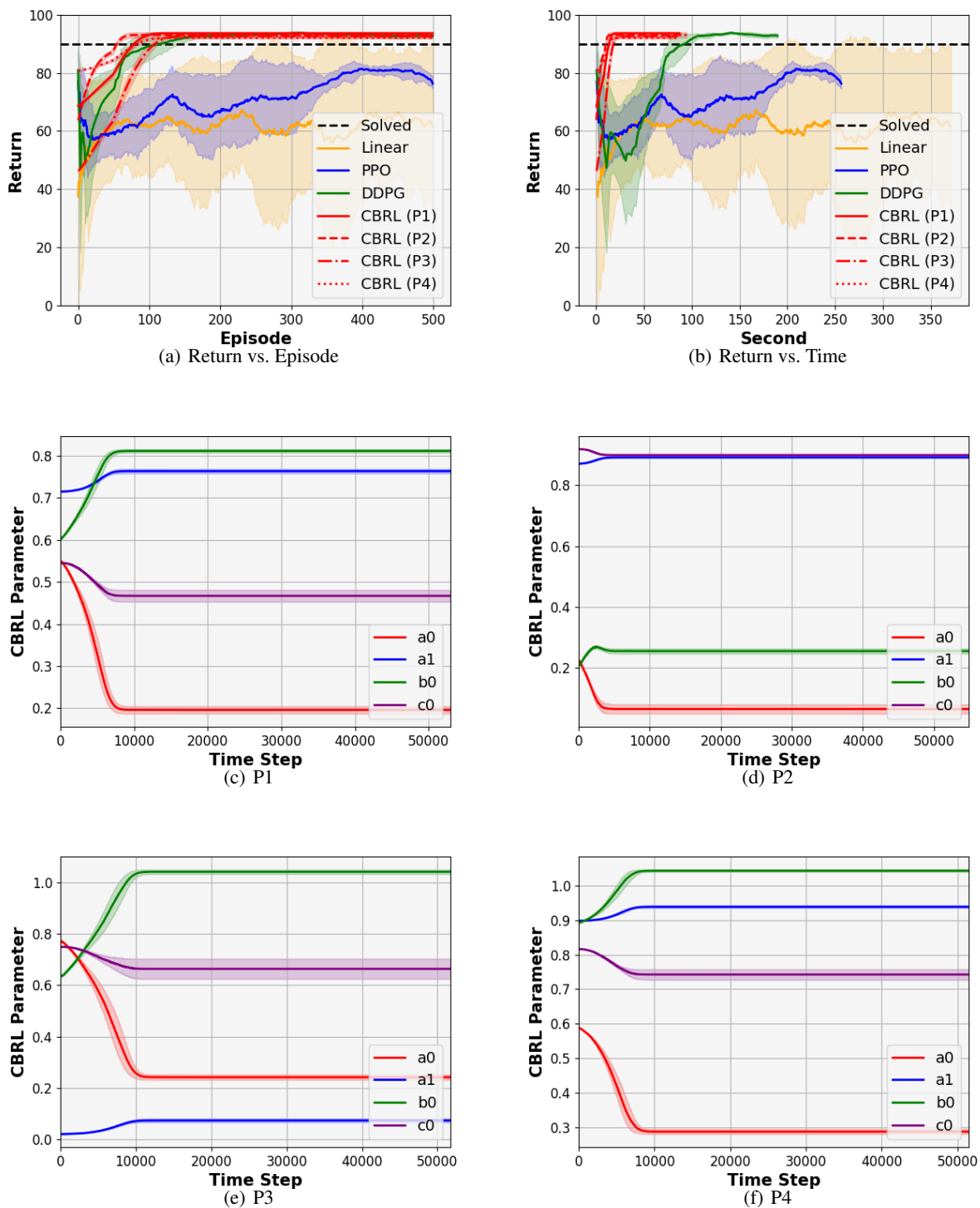


Figure 10: Learning curves of *MountainCarContinuous-v0* over five independent runs. The solid line shows the mean and the shaded area depicts the standard deviation. (a) and (b): Return vs. number of episodes and running time, respectively, for our CBRL approach (over the five independent runs and the four initializations in Table 6) in comparison with the Linear policy, PPO, and DDPG (over the five independent runs). (c) – (f): Learning behavior of CBRL parameters, initialized by Table 6.

Pendulum under CBRL Piecewise-LQR

Environment. As depicted in Figure 11 and described in the main body of the paper, *Pendulum* consists of a link attached at one end to a fixed point and the other end being free, with the goal of swinging up to an upright position by applying a torque on the free end. The state of the system is given by $x = [\theta, \dot{\theta}]$ in terms of the angle of the link θ and the angular velocity of the link $\dot{\theta}$.

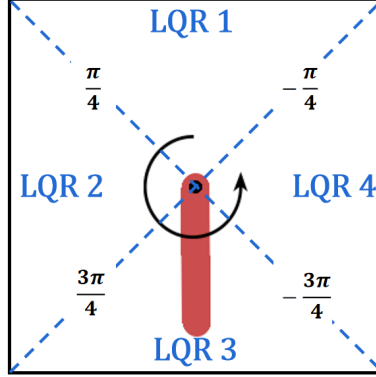


Figure 11: The *Pendulum-v1* environment and partitions for piecewise-LQR.

Controller. Recall that the LQR controller is not sufficient to solve the *Pendulum* problem, even if all the parameters of the system are known (e.g., mass of the link m , length of the link l , moment of inertia of the link J , and gravity g), because a nonlinear controller is required. Consequently, we consider a piecewise-LQR controller that partitions the state space into four regions: LQR 1, LQR 2, LQR 3, LQR 4 (see Figure 11). In terms of the target state $x^* = [\theta^*, \dot{\theta}^*]$, θ^* is selected based on the boundary angle in each partition (counter-clockwise boundary angle if $\dot{\theta} > 0$, and clockwise boundary angle otherwise), while $\dot{\theta}^*$ is selected based on the energy conservation law. More specifically, θ^* in LQR 1 is selected to be $\theta^* = \pi/4$ if $\dot{\theta} > 0$, and to be $\theta^* = -\pi/4$ otherwise. Given the assumption that the link reaches a zero velocity at the upright position, $\dot{\theta}^*$ is selected at any position to be $\dot{\theta}^* = \sqrt{mgl(1 - \cos(\theta))/J}$. We address the problem within the context of our CBRL approach by exploiting the following general matrix form for the piecewise-LQR dynamics

$$\dot{e} = \begin{bmatrix} \dot{\theta} - \dot{\theta}^* \\ \ddot{\theta} - \ddot{\theta}^* \end{bmatrix} = \begin{bmatrix} 0 & 1 \\ a_0 \cos(\theta^*) & a_1 \end{bmatrix} e + \begin{bmatrix} 0 \\ b_0 \end{bmatrix} (u + c_0 \sin(\theta^*)), \quad \dot{\theta}^* = \sqrt{d_0(1 - \cos(\theta))}, \quad (18)$$

which solely takes into account general physical relationships and laws, with the unknown parameters a_0, a_1, b_0, c_0, d_0 to be learned where $e = x - x^*$ and we select $\ddot{\theta}^* = 0$.

Numerical Results. Table 7 and Figure 12 present numerical results for the three state-of-the-art baselines (continuous actions) and our CBRL approach, each run over five independent random seeds. All parameters in (18) are initialized uniformly within $(0, 1)$ and then learned using our control-policy-parameter gradient ascent iteration (6). We consider four sets of initial parameters (see Table 8) to validate the robustness of our CBRL approach. Figure 12(c) – 12(f) illustrates the learning behavior of CBRL parameters given different initialization.

Table 7 and Figure 12(a) and 12(b) clearly demonstrate that our CBRL approach provides far superior performance, in terms of both mean and standard deviation, over all baselines w.r.t. both the number of episodes and running time upon convergence of our CBRL algorithm after a relatively small number of episodes, in addition to demonstrating a more stable training process. More specifically, even with only four partitions for the difficult nonlinear *Pendulum* RL task, our CBRL approach outperforms all baselines after 150 episodes with a significant improvement in mean return over independent random environment runs from Gymnasium (Towers et al. 2023), together with a significant reduction in the standard deviation of the return over these independent runs, thus rendering a more robust solution approach where the performance of each run is much closer to the mean than under the corresponding baseline results. In fact, the relative percentage difference⁴ in improved mean return

⁴For the relative comparison of improved mean return performance of our CBRL method over the next-best RL method, since all the performance values are negative, we use the reversed standard relative percentage difference formula $\frac{|M_{RL} - M_{CBRL}|}{|M_{CBRL}|} \times 100$. Similarly, for the relative comparison of reduced standard deviation of return performance from the next-best RL method to our CBRL method, since all the performance values are positive, we use the standard relative percentage difference formula $\frac{S_{RL} - S_{CBRL}}{S_{CBRL}} \times 100$. Refer to https://en.wikipedia.org/wiki/Relative_change

performance of our CBRL approach over the next-best RL method DDPG (based on mean performance at 500 episodes) is 40% and 53% at 200 and 500 episodes, respectively; and the relative percentage difference in reduced standard deviation of return performance from the next-best RL method DDPG to our CBRL approach is 210% and 263% at 200 and 500 episodes, respectively. Moreover, the relative percentage difference in improved mean return performance of our CBRL approach over the PPO RL method is 197% and 168% at 200 and 500 episodes, respectively; and the relative percentage difference in reduced standard deviation of return performance from the PPO RL method to our CBRL approach is 275% and 793% at 200 and 500 episodes, respectively.

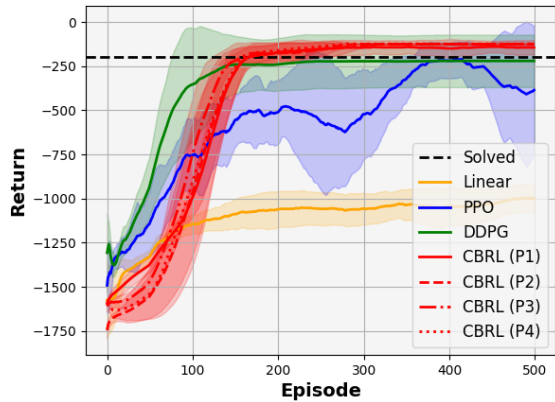
We note an important difference between Figure 4(a),(b) and Figure 12(a),(b), namely the shaded areas in Figure 4(a),(b) represent one form of variability across independent random seeds with the same parameter initialization, whereas the shaded areas in Figure 12(a),(b) represent the combination of two forms of variability – one across independent random seeds with the same parameter initialization and the other across different random parameter initializations.

Table 7: Mean and Standard Deviation of Return of RL Methods for *Pendulum-v1*

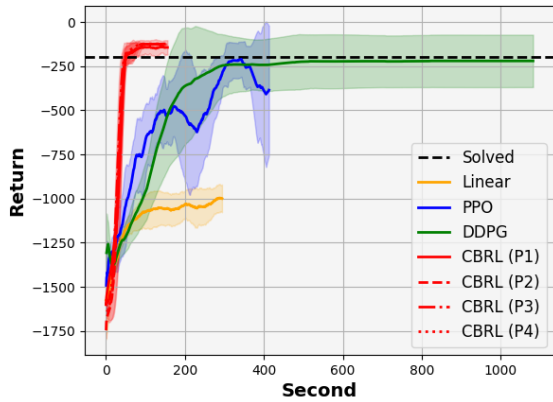
Episode Number	CBRL		Linear		PPO		DDPG	
	Mean	Std. Dev.	Mean	Std. Dev.	Mean	Std. Dev.	Mean	Std. Dev.
50	-1378.78	43.89	-1331.73	36.25	-1147.35	181.20	-942.18	170.83
100	-1004.75	101.66	-1145.30	53.57	-757.11	205.66	-355.09	324.16
150	-284.26	130.17	-1088.67	83.73	-559.65	151.39	-241.16	162.85
200	-172.48	48.32	-1062.06	102.63	-511.85	181.28	-240.94	149.57
250	-152.80	37.43	-1058.88	92.55	-561.78	384.15	-222.18	151.71
300	-145.56	44.16	-1057.02	90.29	-524.10	259.46	-221.78	150.40
350	-141.80	36.63	-1036.65	88.37	-325.66	133.77	-222.83	146.68
400	-149.34	51.70	-1044.34	100.90	-218.37	100.83	-220.28	148.80
450	-139.65	32.36	-1032.82	87.11	-296.94	184.32	-220.50	148.68
500	-143.95	40.91	-999.41	78.75	-385.50	365.39	-220.38	148.54

Table 8: Initial Parameters of *Pendulum-v1*

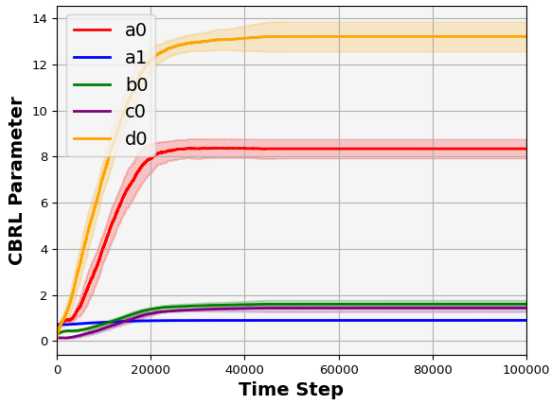
Name	a_0	a_1	b_0	c_0	d_0
Initial Parameters 1 (P1)	0.417	0.72	0.302	0.147	0.092
Initial Parameters 2 (P2)	0.893	0.332	0.821	0.042	0.108
Initial Parameters 3 (P3)	0.18	0.019	0.463	0.725	0.42
Initial Parameters 4 (P4)	0.223	0.523	0.551	0.046	0.361



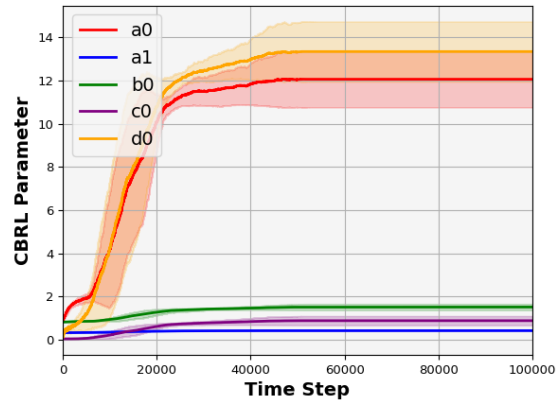
(a) Return vs. Episode



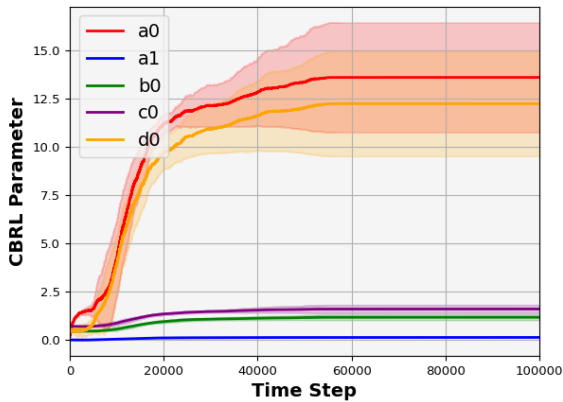
(b) Return vs. Time



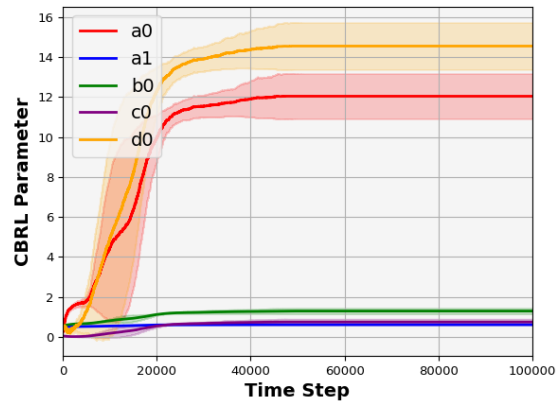
(c) P1



(d) P2



(e) P3



(f) P4

Figure 12: Learning curves of *Pendulum-v1* over five independent runs. The solid line shows the mean and the shaded area depicts the standard deviation. (a) and (b): Return vs. number of episodes and running time, respectively, for our CBRL approach (over the five independent runs and the four initializations in Table 8) in comparison with the Linear policy, PPO, and DDPG (over the five independent runs). (c) – (f): Learning behavior of CBRL parameters, initialized by Table 8.

Implementation

Baselines. As previously noted, the evaluation of our CBRL approach includes comparisons against the three baselines of DQN for discrete actions, DDPG for continuous actions and PPO, which are selected as the state-of-the-art RL algorithms for solving the RL tasks under consideration. The additional baseline of replacing the nonlinear policy of PPO with a linear policy was again included because the optimal policy for some problems, e.g., *Cart Pole*, is known to be linear. This Linear algorithm solely replaces the policy network of PPO with a linear policy while maintaining all other components unchanged. More specifically, we decrease the number of hidden layers in the policy network by 1, reduce the hidden layer size of the policy network to 16, and remove all (nonlinear) activation functions in the policy network.

Hyperparameters. We summarize in Table 9 the hyperparameters that have been used in our experiments. To ensure a fair comparison, we maintain consistent hyperparameters (e.g., hidden layer size of the value network and the activation function) across all algorithms wherever applicable.

Table 9: Summary of Experimental Hyperparameters

Algorithm	Linear	PPO	DDPG	DQN	CBRL
Action Generator	NN	NN	NN	NN	CBRL-LQR
# of Hidden Layers (Policy)	1	2	2	2	N/A
# of Hidden Layers (Value)	2	2	2	2	2
Hidden Layer Size (Policy)	16	128	128	128	N/A
Hidden Layer Size (Value)	128	128	128	128	128
Activation (Policy)	N/A	ReLU & Tanh	ReLU & Tanh	ReLU & Tanh	N/A
Activation (Value)	ReLU	ReLU	ReLU	ReLU	ReLU
Discount Factor	0.99	0.99	0.99	0.99	0.99
Clip Ratio	0.2	0.2	N/A	N/A	N/A
Soft Update Ratio	N/A	N/A	0.005	N/A	N/A

Computing Infrastructure. All experiments in this work were implemented and executed on an 8G-memory Macbook Air with a M1 Chip.